

Large-Eddy Simulation Study of the Effects on Flow of a Heterogeneous Forest at Sub-Tree Resolution

Fabian Schlegel · Jörg Stiller · Anne Bienert ·
Hans-Gerd Maas · Ronald Queck ·
Christian Bernhofer

Received: 11 November 2013 / Accepted: 2 August 2014 / Published online: 31 August 2014
© Springer Science+Business Media Dordrecht 2014

Abstract The effect of three-dimensional plant heterogeneity on flow past a clearing is investigated by means of large-eddy simulation. A detailed representation of the canopy has been acquired by terrestrial laser scanning for a patch of approximately 328 m length and 172 m width at the field site “Tharandter Wald”, near the city of Dresden, Germany. The scanning data are used to produce a highly resolved, three-dimensional plant area distribution representing the actual canopy. Hence, the vegetation maintains a rich horizontal and vertical structure including the three-dimensional clearing. The scanned plant area density is embedded in a larger domain, which is filled with a heterogeneous forest generated by the virtual canopy generator of Bohrer et al. (Tellus B 59:566–576, 2007). Based on forest inventory maps and airborne laser scanning, the characteristics of the actual canopy are preserved. Furthermore, the topography is extracted from a digital terrain model with some modifications to accommodate for periodic boundary conditions. A large-eddy simulation is performed for neutral atmospheric conditions and compared to simulations of a two-dimensional plant area density and an one-year-long field experiment conducted at the corresponding field site. The results reveal a considerable influence of the plant heterogeneity on the mean velocity field as well as on the turbulent quantities. The three-dimensional environment, e.g., the oblique edges combined with horizontal and vertical variations in plant area density and the topography create a sustained vertical and cross-flow velocity. Downstream of the windward forest edge an enhanced gust zone develops, whose intensity and relative position are influenced by the local canopy density and, therefore, is not constant along the edge. These results lead

F. Schlegel (✉) · J. Stiller
Institute of Fluid Mechanics, Technische Universität Dresden, 01062 Dresden, Germany
e-mail: fabian.schlegel@tu-dresden.de

A. Bienert · H.-G. Maas
Institute of Photogrammetry and Remote Sensing,
Technische Universität Dresden, 01062 Dresden, Germany

R. Queck · C. Bernhofer
Institute of Hydrology and Meteorology, Technische Universität Dresden,
01062 Dresden, Germany

us to the conclusion that the usage of a three-dimensional plant area distribution is essential for capturing the flow features inside the canopy and within the mixing layer above.

Keywords Edge flow · Forest canopy · Heterogeneous vegetation · Large-eddy simulation · Terrestrial laser scanning · Turbulence

1 Introduction

Interaction between plant canopies and the atmospheric boundary layer is of considerable interest for a broad range of applications, e.g., meteorology, agriculture or biology. With the pioneering work of Inoue (1955) on the “Honami” effect—wave-like motions observed in wheat crops on windy days—a process of understanding the fundamental transport mechanisms was started. For a general overview on canopy flows we refer to the comprehensive surveys of Raupach and Thom (1981), Finnigan (2000), de Langre (2008) and Patton and Finnigan (2012). Here we focus on tall vegetation, in particular a forest stand typical for central and western Europe.

In such forests heterogeneity of the vegetation is omnipresent and complicates the interpretation of measurements. The ramified structure and random distribution of plants inside a forest stand pose a notorious problem to the modelling of canopy flows. Except for isolated trees (Endalew et al. 2009, 2011), fractal plant models (Chester and Meneveau 2007; Schröttele and Dörnbrack 2013) and groups of a few trees (Graham and Meneveau 2012) consideration of detailed plant morphology remains beyond the reach of numerical simulations.

On a larger scale, abstraction from structural diversity, flexibility and elasticity appears to be mandatory and leads to a characterization of the canopy using a plant area density (*PAD*). Vertical integration yields an even more condensed measure, the plant area index (*PAI*). By introducing an isotropic drag coefficient, *PAD* is related to the aerodynamic resistance caused by the vegetation. In addition, the interaction of turbulent scales and plants has to be considered separately using an adapted turbulence model (Shaw and Pereira 1982; Wilson 1988; Katul et al. 2004; Sogachev 2009; Lopes et al. 2013) or subgrid-scale model (Shaw and Schumann 1992; Shaw and Patton 2003). Under certain conditions, and as a further simplification, a forest stand can be considered as horizontally homogeneous. The flow above such quasi-homogeneous canopies has been investigated extensively in laboratory and field experiments, as well as in numerical simulations (Gao et al. 1989; Raupach et al. 1996; Brunet and Irvine 2000; Fitzmaurice et al. 2004; Dupont and Brunet 2006, 2008c; Juang et al. 2008; Panferov and Sogachev 2008; Finnigan et al. 2009; Iwata et al. 2009; Watanabe 2009; GavriloV et al. 2011; Patton et al. 2011; Poggi et al. 2011; Serafimovich et al. 2011; Sogachev et al. 2011; Edburg et al. 2012; Huang et al. 2013; Júnior et al. 2013).

Of course, uniform canopies are rather the exception than the rule. Heterogeneity results, for example, from the transition between forested and grassy patches, from topography and from plant diversity and distribution inside the stands themselves. The flow across a forest edge represents a generic model of the first type of heterogeneity, which is usually simplified by assuming vegetation as horizontally homogeneous. Much work has been devoted to this particular type of canopy flow, e.g., the field and laboratory experiments of Raynor (1971), Irvine et al. (1997), Novak et al. (2000), Morse et al. (2002), Detto et al. (2008), Kochendorfer and Paw U (2011), Eder et al. (2013) and Fontan et al. (2013), or the numerical simulations of Lee (2000), Sogachev et al. (2008), Dalpé and Masson (2009), Dupont and Brunet (2009) and Fesquet et al. (2009). A main effect is a strong distortion of the flow at the windward edge, triggering the development of an enhanced gust zone further downstream inside the forest

stand (Raupach et al. 1987; Yang et al. 2006a, b; Dupont and Brunet 2008a). Consideration of risk assessment due to windbreaks is consequently of particular interest (Yang et al. 2006c; Dupont and Brunet 2008b; Ruck et al. 2012). If the forest stand is characterized by an open trunk space with sparse understorey, a sustained sub-canopy jet develops across the windward edge that contributes to the energy and mass exchange and establishes a second mixing layer below the crown section (Dupont and Brunet 2008a; Dupont et al. 2011, 2012). The flow at the leeward edge of a forest is dominated by an intermittent separation zone that forms in the forest interior and on the clearing (Cassiani et al. 2008). Its intensity and dimensions are influenced by the canopy density of the upstream forest and the relative length of the clearing itself (Frank and Ruck 2008).

Today, many forested areas lie within hilly or mountainous terrain (Ross and Vosper 2005), thus introducing another type of heterogeneity to the vegetation, which is caused indirectly by the topography. As the mean flow penetrates the windward canopy of a forested hill from aloft this contribution has to be taken into account for the energy and mass transport (Ross 2008). The distinct features of a forested hill have been investigated within several laboratory experiments, e.g., Finnigan and Brunet (1995), Poggi and Katul (2007a, b, c) and Poggi et al. (2007), or numerical simulations, e.g., Katul et al. (2006), Dupont et al. (2008), Patton and Katul (2009) and Ross (2011). Recently, Ross and Baker (2013) presented a partially forested hill as a combination of the two types of heterogeneity. Noteworthy is also the extensive work on analytical descriptions of the flow across a forested hill undertaken by, e.g., Finnigan and Belcher (2004), Belcher et al. (2008, 2012), Poggi et al. (2008), Harman and Finnigan (2010, 2013) and Wang and Yi (2012).

However, our main interest is dedicated to inhomogeneity resulting from plant diversity and distribution inside the forest stand itself. At length scales of the crown diameter and the crown-base height the individual properties with regard to the plant and leaf area distribution between the neighbouring trees becomes relevant. First work on the modelling of small-scale plant heterogeneity in numerical simulations has emerged recently, e.g., Bohrer et al. (2007, 2008, 2009), Yue et al. (2007), Schlegel et al. (2012) and Bailey and Stoll (2013). Ross (2012) presented the first analytical approach that is, however, limited to a slowly varying *PAD*. Bohrer et al. (2009) demonstrated the feasibility of using a heterogeneous *PAD* by means of large-eddy simulation (LES). They used a virtual canopy generator to generate a three-dimensional canopy based on patch maps and spatial autocorrelations of observed properties (Bohrer et al. 2007). By studying different scenarios (winter vs. spring, heterogeneous vs. patchy), Bohrer et al. (2009) conclude that the small-scale plant heterogeneity decreases the displacement height and increases the roughness length to be used in regional models. As another result, hot spots of sweeps and ejections develop, which can affect local gas exchange and particle transport (Bohrer et al. 2008). Using terrestrial laser scans, Schlegel et al. (2012) presented the first LES study in which a realistic fine-scale plant heterogeneity derived directly from a real forest was considered. Their results revealed a significant influence on the turbulent flow field, particular near edges.

The intention of the present study is to consider a highly resolved, three-dimensional and realistic representation of vegetation in a numerical simulation. The article is organized as follows: in Sect. 2 we introduce our numerical method, and Sect. 3 presents a description of the field site and the field experiment TurbEFA. We review the method of terrestrial laser scanning, together with the adapted virtual canopy generator of Bohrer et al. (2007), which is used to extend the measured *PAD*. For the first time within a numerical simulation a three-dimensionally shaped forest edge surrounding the clearing is considered. Additionally a digital terrain model is included at the lower boundary. The results are discussed in Sect. 4 and compared to the field measurements; in addition we determine the influence of a small-

scale plant heterogeneity on the mean flow and the turbulent quantities, e.g., location and intensity of an enhanced gust zone. Finally, conclusions are presented in Sect. 5.

2 Numerical Method

For the present LES study we restrict ourselves to neutral atmospheric conditions. Furthermore, the computational domain has to be large enough to allow for evolution of the dominant coherent structures and the roughness sublayer, which requires a domain size of the order of 1 km² for a typical forest in central and western Europe (Su et al. 2000; Yang et al. 2006a, b). Under these conditions variations in density and the influence of the Coriolis force can be neglected (Lumley and Panofsky 1964).

The basic idea behind LES is to distinguish between the energy-carrying, resolved scales and the unresolved, subgrid scales of motion by using a filter operation (Sagaut 1998; Pope 2000). Application of the filter to the Navier-Stokes equations yields the resolved scale or LES equations

$$\partial_t \bar{u}_i + \partial_j (\bar{u}_j \bar{u}_i) = -\partial_i \bar{p} + \partial_j (2\nu \bar{S}_{ij}) + \partial_j \tau_{ij} + \bar{f}_{i,d} + \bar{f}_{i,p}, \tag{1a}$$

$$\partial_i \bar{u}_i = 0, \tag{1b}$$

where \bar{u} is the resolved velocity, \bar{p} is the resolved pressure divided by density and ν is the kinematic viscosity ($1.46 \times 10^{-5} \text{ m}^2 \text{ s}^{-1}$ for air at 15 °C). An uniform pressure gradient $\bar{f}_{i,p}$ is added for maintaining a prescribed bulk velocity in the presence of periodic boundary conditions.

The effect of the subgrid scales is represented within Eq. 1 by the so-called subgrid-scale (SGS) stresses $\tau_{ij} = -(\overline{u_i u_j} - \bar{u}_i \bar{u}_j)$ (Lilly 1967), and related to the strain rate tensor \bar{S}_{ij} using the Boussinesq approach

$$\tau_{ij} = 2\nu_r \bar{S}_{ij} - \frac{2}{3} \delta_{ij} \bar{k}''', \tag{2}$$

where $\nu_r = C_v \ell \bar{k}'''^{1/2}$ is the subgrid-scale viscosity. For closure a SGS model is required. Basically, it uses the transport equation for the unresolved turbulent kinetic energy \bar{k}''' according to Deardorff (1980) with extensions for canopy flows introduced by Shaw and Schumann (1992)

$$\partial_t \bar{k}''' + \partial_j (\bar{u}_j \bar{k}''') = \tau_{ij} \bar{S}_{ij} + \partial_j (2\nu_r \partial_j \bar{k}''') - C_E \frac{\bar{k}'''^{3/2}}{\ell} - \frac{2\bar{k}'''}{\tau}. \tag{3}$$

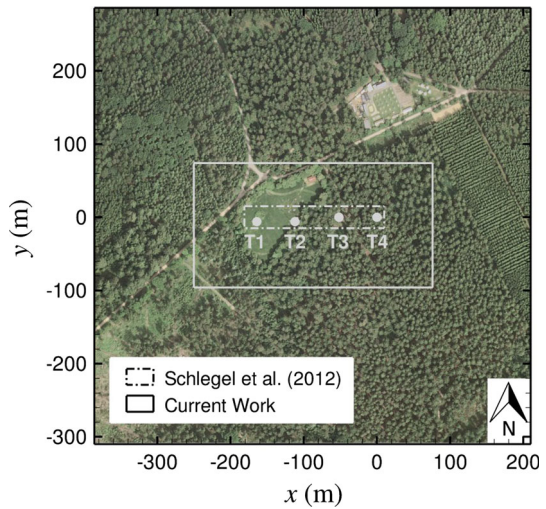
The last term mimics the spectral short-cut associated with the enhanced energy removal in the wake of plant parts (Kaimal and Finnigan 1994) and contains a time scale $\tau = \bar{u}_i / \bar{f}_{i,d}$ for this bypass effect. The approach was recently confirmed by Shaw and Patton (2003).

Thom (1975) showed that the pressure forces caused by the canopy exceed the viscous forces, and, due to this, the latter are neglected. Following the approach of Shaw and Schumann (1992) we model the canopy drag force as the product of local wind speed $|\bar{\mathbf{u}}|$, a single-side value of PAD, a , and an effective drag coefficient c_d including shelter and lee effects (Raupach and Thom 1981),

$$\bar{f}_{i,d} = -c_d a |\bar{\mathbf{u}}| \bar{u}_i. \tag{4}$$

Following Shaw et al. (1988) the drag coefficient c_d is assumed to be 0.15. The remaining constants are chosen according to Schmidt and Schumann (1989), i.e., $C_v = 0.0857$ and $C_E = 0.845$.

Fig. 1 Orthophoto of the investigated domain. The *solid* and *dashed frames* mark the area with available terrestrial laser scanning data in the current work compared to preliminary work of Schlegel et al. (2012). Additionally the positions of the four measurement towers T1–T4 are marked by *dots*. Orthophoto ATKIS®-DOP © Staatsbetrieb Geobasisinformation und Vermessung Sachsen 2013



The LES equations (1, 3) are discretized by a semi-implicit, cell-centred finite-volume method of second-order accuracy. The model is implemented in the OpenFoam® CFD toolbox in version 2.1 (Jasak 1996; Weller et al. 1998). Details about the numerical method and validation are presented elsewhere (Schlegel et al. 2012).

3 Field Study

3.1 Description of Field Site

The subject of investigation is a field site located about 25 km south-west of the city of Dresden in Germany. Surrounded by the forest “Tharandter Wald” the site accommodates a micrometeorological station founded in 1958 and a 42-m high permanent scaffolding tower (T4), which has been continuously operated by the Institute of Hydrology and Meteorology of Technische Universität Dresden since 1996.

The forest stand was seeded in 1887 and is today dominated by *Picea abies* (about 72%, based on forest assessments in 1999 and 2004). For more details on the composition of the vegetation we refer to Feigenwinter et al. (2004), Grünwald and Bernhofer (2007) and Queck et al. (2012). The “Tharandter Wald” shows the typical features of a managed forest, and is characterized by a dense canopy and an open trunk space with a sparse understorey. Next to tower T4 the mean tree height is estimated to be 30 m and the single-side PAI $\approx 7.1 \text{ m}^2 \text{ m}^{-2}$ (Queck and Bernhofer 2010).

As is commonly known for forested areas in central and western Europe, homogeneity is rather the exception than the rule (Bernhofer et al. 2003). Hence, it is no surprise that scrutiny of the aerial photography in Fig. 1 reveals large inhomogeneities within the investigated domain, which extends along the predominant wind direction from west to east (Queck et al. 2012). The most prominent feature is a 50 m \times 90 m clearing called “Wildacker”. Due to its location approximately 100 m upstream of tower T4, it has a significant influence on tower measurements. The “Wildacker” is surrounded by a belt of *Castanea sativa* closing the trunk space and smoothing the windward forest edge. Furthermore, large inhomogeneities

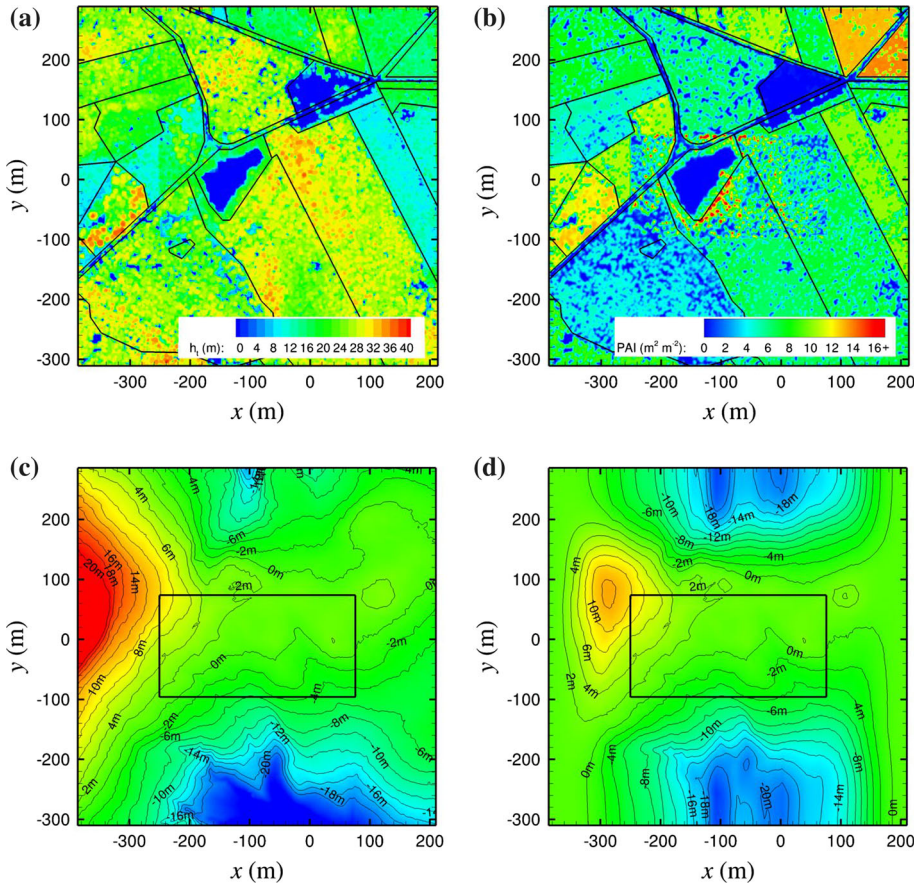


Fig. 2 *Top*: canopy height (a) and PAI (b) for the investigated domain obtained from the combination of terrestrial laser scanner data and the virtual canopy generator of Bohrer et al. (2007). The black solid lines mark the forest plots. *Bottom* original topography (c) obtained from the digital terrain model ATKIS®-DGM2 and the modified version (d) for usage with periodic boundary conditions. The black solid frame indicates the central region, where the terrain height is not modified. ATKIS®-DGM2 © Staatsbetrieb Geobasisinformation und Vermessung Sachsen 2013. **a** Canopy height with marked forest plots. **b** PAI with $2\text{ m} \times 2\text{ m}$ filter width. **c** Original topography. **d** Modified topography

are visible towards north and south, including in particular an ecological measurement field, a young spruce plantation and forest trails.

To account for the inhomogeneity and to allow for a better characterization of the vegetation, the investigated domain is decomposed into 29 forest plots marked in Fig. 2a. Within each plot randomly distributed measurements were carried out to yield information about mean tree height and mean PAI. The latter was measured with a Li-Cor LAI 2000 plant canopy analyzer and corrected according to Chen and Black (1991), giving values between 3.8 and $14.1\text{ m}^2\text{ m}^{-2}$. The mean tree height of the forest plots varies between 7.5 and 33 m .

3.2 Field Experiment

The study uses observations from the TurbEFA field campaign carried out from May 2008 to May 2009. High frequency samples of the wind vector were obtained by ultrasonic anemome-

ters mounted on four towers and various ground-level positions along a transect pointing towards the west from tower T4. The detailed description of set-up, mounting of the ultrasonic anemometers and post-processing is discussed in [Schlegel et al. \(2012\)](#).

Figure 1 shows the tower positions along the transect, which covers the forest-clearing interface. Approximately 100 m eastward of the clearing stands the 42-m high permanent scaffolding tower T4. Towards the west it was succeeded by two temporarily constructed scaffolding towers of 40-m height. Tower T3 was placed inside the forest stand and tower T2 on the clearing, right beside the eastward forest edge. Additionally, a 30-m high telescoping tower T1 was erected at the westerly end of the “Wildacker”.

In general, flow from the west (wind sector: 255° – 285° , 12% of the time during the measurement campaign) is investigated, since this is the predominant wind direction. Furthermore, we constrain ourself to neutral conditions. The stability index $\zeta = z/L$, where L is the Obukhov length ([Monin and Obukhov 1954](#)), is confined to ± 0.1 and is based on measurements at a height of 42 m on the main tower T4. Finally, the comparison of the results of the field study with the numerical simulation is based on more than 8000h of wind-field data.

3.3 Terrestrial Laser Scanning

Terrestrial laser scanning is an efficient three-dimensional measurement method with an increasing range of application fields, e.g., acquisition of forest inventory parameters ([Aschoff and Spiecker 2004](#); [Maas et al. 2008](#); [Vosselman and Maas 2010](#)). Within the scope of the present study, we give only a brief introduction of the scanning procedure and how to derive *PAD* values from the unorganized point cloud.

The preferred multiple-scan method requires scans from various predefined ground positions and a geometric registration within a common coordinate system ([Bienert and Maas 2009](#)). To derive the desired *PAD* values, the joint point cloud is converted into a corresponding voxel¹ space by application of a ray-tracing method. By that, each voxel is associated with a reflection probability, that, augmented by a plant specific clumping factor, determines *PAD* values ([Bienert et al. 2010](#)). The unknown factor is derived by comparison of the integral sum of the reflection probability and the known $PAI = 7.1 \text{ m}^2 \text{ m}^{-2}$ inside an area adjacent to the permanent scaffolding tower T4 ([Queck et al. 2012](#)).

In [Schlegel et al. \(2012\)](#), the forest stand was represented by approximately 50×10^6 points obtained by scans from 13 different ground positions, including one at the top of the permanent scaffolding tower T4. Unfortunately, availability of reliable data was restricted to a strip of 30 m width and 191 m length, which includes the clearing in the x -direction but not in the y -direction (dashed frame marked in Fig. 1). Therefore, simplified *PAD* values averaged in the y -direction were used. To overcome this restriction, additional scans were carried out in autumn 2011, yielding a more detailed representation comprising approximately 150×10^6 points. In total, scans from 25 different ground positions are available, including two at the top of scaffolding towers T2 and T4. In conjunction with a more elaborated post-processing of the joint point cloud, a realistic three-dimensional *PAD* was devised for an area of $328 \text{ m} \times 172 \text{ m}$ (solid frame marked in Fig. 1). This includes not only an enlargement towards north and south to cover the forest stand beside the clearing, but also a larger region upstream of the clearing and downstream of the permanent scaffolding tower T4.

¹ A voxel is the three-dimensional equivalent of a pixel, i.e., a rectangular volume element with its faces aligned parallel to the coordinate axes.

3.4 Virtual Canopy Generator

The required scanning area matching for the LES of a canopy flow with a characteristic mean tree height of $h_{\text{ref}} = 30$ m would be around 0.36 km^2 (see Sect. 4.1 for details), which would include an unrealistic large scanning effort considering the occlusion-induced range limitations of a terrestrial laser scanner in a forest. As a remedy, Bohrer et al. (2007) presented a “virtual canopy generator” for building a heterogeneous forest that preserves the mean biophysical features of the forest stand, although differing from reality when considering explicit fine details. Having in mind that 95 % of the German forests are managed (Bundesministerium für Ernährung, Landwirtschaft und Verbraucherschutz 2009), various statistical data, obtained for each of the 29 forest plots, are available, e.g., mean tree height, diameter at breast height or *PAI* values. Using these as input, the virtual canopy generator is set up to create a local *PAI* on an equidistant, orthogonal mesh of 2-m resolution for the whole computational domain. The three-dimensional canopy volume is then filled by applying generic profiles for the *PAD*, which are based on Peters and Eiden (1992) and Kraus (2008).

The generation of the virtual canopy proceeds as follows: firstly, the canopy has to be decomposed into a given number of patches, which can be done by distinguishing between characteristic canopy properties, e.g., plant species into trees and grass, or regional subdivisions such as the aforementioned forest plots. Henceforth, all the following operations are performed patchwise. Furthermore, a so-called random canopy field has to be provided for every patch/plot to prescribe a horizontal structure of the contained vegetation. Various possibilities can be found in Bohrer et al. (2007), but as an area-wide high resolution digital canopy height model exists, this is used directly (G. Bohrer, personal communication, 2014). It is based on the digital terrain model ATKIS[®]-DGM2 (see Sect. 3.5 for details), because the terrestrial laser scanning data are not available for the whole computational domain. Therefore, the airborne raw data are used to generate a digital surface model, from which the local terrain height is subtracted. Finally, we obtain a digital canopy height model, and, by this, a local tree height h_t with the required resolution of 2 m (Bienert et al. 2011). Bohrer et al. (2007) showed that a simple transformation based on a normalization of the random canopy field N , the observed mean values $\langle \cdot \rangle^{\text{obs}}$ and their standard deviation σ^{obs} allow the generation of a heterogeneous two-dimensional field preserving the mean biophysical features within every patch,

$$PAI = \langle PAI \rangle^{\text{obs}} + N_{h_t} \sigma_{PAI}^{\text{obs}}. \quad (5)$$

Note that all equations are written in terms of *PAI* values as the desired quantity and the digital canopy height model as a random canopy field. The mean *PAI* for every patch is derived from local measurements (Sect. 3.1); thus, the normalized field is calculated from

$$N_{h_t} = \frac{h_t - \langle h_t \rangle}{\sigma_{h_t}}. \quad (6)$$

The canopy of the whole computational domain is composed by adding up the patchwise generated fields and the *PAD* values within the three-dimensional canopy volume are calculated from generic profiles with the generated *PAI* and the known tree height h_t . Last, but not least, the virtual forest is replaced by the observed forest where terrestrial laser scanning data are available. Figure 2a, b shows the tree height and the *PAI* of the canopy as a combination of both methods.

3.5 Topography

As is typical of the German mid-range mountains the field site is characterized by a gently wavy terrain, revealing depressed areas northward and southward, and a 30-m hill upstream of the anchor station (Fig. 2c). Taken from the high-resolution digital terrain model ATKIS[®]-DGM2² and gained by airborne laser scanning with a Riegl LMS-Q560 laser scanner, the terrain information has a resolution of 2 m and a precision of ± 0.2 m.

The usage of the original ATKIS[®]-DGM2 data would require open boundary conditions, many of which are related to the Sommerfeld radiation condition, e.g., [Orlanski \(1976\)](#), but all demand a predominant inflow or outflow in terms of a known phase velocity. For the lateral boundaries simultaneous inflow and outflow are expected due to the terrain level, which is beyond the possibilities of this type of boundary condition. The best choice is horizontal periodicity, having also the advantage of a natural turbulence power spectrum for the inflow.

Nevertheless, this requires a smoothing of the original ATKIS[®]-DGM2 data at opposite boundaries such that the corresponding points on either side are located at the same height, denoted as h_0 . To change as little as possible, a central region coinciding with the terrestrial laser scanning data was fixed and the adjustment is conducted only within a surrounding strip. The black solid frame in Fig. 2c, d indicates the central region, with the lower left corner located at $x = -251$ m, $y = -97$ m, and the upper right at $x = 77$ m, $y = 75$ m. The coordinates are given with respect to tower T4.

The smoothing is achieved by an one-dimensional weighted average between the original terrain height h_1 and the target height h_0 . We apply the averaging successively from north to south (lateral) and then from west to east (streamwise). For both sides of each direction a modified terrain height is calculated as follows,

$$h(\xi) = [1 - w(\xi)] h_1(\xi) + w(\xi) h_0, \quad (7)$$

with ξ as a normalized coordinate ranging between $0 \leq \xi \leq 1$, with $\xi = 0$ indicating the boundary and $\xi = 1$ the beginning of the central region. The weighting function

$$w(\xi) = \frac{(1 - \xi)^2}{(1 - \xi)^2 + \xi^2} \quad (8)$$

ensures a smooth transition without sharp edges due to a zero gradient at $\xi = 0$ and $\xi = 1$. The target height varies between the application in the lateral and streamwise directions. In the first case the target height is calculated from the mean value of the original height of the two opposite points, and in the second case the mean height of the central area of 0.7 m was taken as a constant target height, resulting in a plateau at the inflow and outflow boundaries. The result of the smoothing is shown in Fig. 2d, and taken as grid points for the bottom boundary of the computational domain.

4 Results

4.1 Overview

[Schlegel et al. \(2012\)](#) demonstrated the feasibility of using terrestrial laser scanning data for canopy flows. Despite the partially homogeneous forest and a laterally-averaged, measured

² ATKIS[®]-DGM2 is provided by Staatsbetrieb Geobasisinformation und Vermessung Sachsen (www.landesvermessung.sachsen.de).

PAD, the simulations revealed a significant influence of the small-scale plant heterogeneity on the turbulent flow field compared to a piecewise homogeneous forest. The present intention is to overcome most of the previous limitations and to include a three-dimensional virtual forest into a LES, representing a particular field site. The heterogeneous *PAD* within the central region is derived from terrestrial laser scanning (Sect. 3.3), and for the remaining part by the application of the virtual canopy generator (Sect. 3.4).

The dimensions of the computational domain are based on the conclusions of Yang et al. (2006a, b). They suggested a length of $20 h_{\text{ref}}$ for the horizontal and $6 h_{\text{ref}}$ for the vertical direction, where h_{ref} denotes in our case to the nominal tree height of 30 m. These limits should allow an adjustment of the flow downstream of a forest edge and accommodate the development of dominant coherent structures (Finnigan 2000; Dupont and Brunet 2009; Finnigan et al. 2009). Above the canopy, the development of the well-known roughness sub-layer extending towards $3 h_{\text{ref}}$ (Raupach and Thom 1981) dictates the height of the domain. Adopting the aforementioned criteria we construct a computational domain of $600 \text{ m} \times 600 \text{ m} \times 240 \text{ m}$. In contrast to Yang et al. (2006a, b) we increased the domain height by $2 h_{\text{ref}}$ to account for possible terrain effects. The given value represents the minimum height of the domain at the highest point. Tower T4 represents the origin of the coordinate system with a streamwise x -, a lateral y - and a vertical z -axis. The central region containing the measured *PAD* and the real topography starts at $x = -251 \text{ m}$, $y = -97 \text{ m}$ and ends at $x = 77 \text{ m}$, $y = 75 \text{ m}$. Since it is placed in the middle of the computational domain the origin moves towards the north-west about 387 m away from the inflow, and 311 m away from the southward lateral boundary.

All computations are performed using periodic boundary conditions for the horizontal directions. At the bottom a no-slip condition together with the logarithmic velocity law for rough walls using a roughness length of $z_0 = 0.02 \text{ m}$ (Schlichting and Gersten 2000) is imposed and at the top we use a free-slip condition. As a consequence of the topography, the mesh becomes non-orthogonal and non-equidistant. Applying an average mesh spacing of 2 m yields 302×300 grid cells in the z -plane and between 120 and 132 in the vertical. Due to non-orthogonality and a variable grid spacing an additional mapping has to be applied between the orthogonal voxel spaces and the numerical mesh, by calculating the mean value of the *PAD* over those voxels, whose centre points are located inside each grid cell. Once the computational domain and the virtual forest are defined, we have to prescribe a flow regime. To fit the measurement window of the field study, the mesoscale pressure forcing term $\bar{f}_{i,p}$ was adjusted to achieve a mean wind speed of $\approx 4 \text{ m s}^{-1}$ at a height of 42 m above ground at tower T4.

Time integration was performed over a period of 11,100 s with a timestep of 0.1 s. For statistical computations we stored snapshots of the instantaneous velocity field at a rate of 0.5 Hz over the last 3,600 s of the computational run and mean values (angular brackets), fluctuations (prime) and higher-order statistics, e.g., skewness, were computed afterwards. The corresponding decomposition of the filtered velocity is

$$\bar{u}_i = \langle \bar{u}_i \rangle + \bar{u}'_i. \quad (9)$$

For ease of analysis and to simplify the notation we introduce the following dimensionless quantities:

– horizontal and vertical positions

$$X = x/h_{\text{ref}}, \quad (10a)$$

$$Y = y/h_{\text{ref}}, \quad (10b)$$

$$Z = z/h_{\text{ref}}, \quad (10c)$$

Table 1 Tower positions within the computational domain. Coordinates are normalized according to Eq. 10

| | T1 | T2 | T3 | T4 |
|---|-------|-------|-------|-----|
| X | -5.47 | -3.73 | -1.73 | 0.0 |
| Y | -0.2 | -0.2 | 0.0 | 0.0 |

– velocity

$$U_i = \langle \bar{u}_i \rangle / U_{\text{ref}}, \tag{11a}$$

$$U'_i = \bar{u}'_i / U_{\text{ref}}, \tag{11b}$$

where U_{ref} represents the mean wind speed at a height of 42 m above ground on tower T4. More specifically we denote the mean streamwise and vertical components as $U = U_1$, $V = U_2$ and $W = U_3$, respectively.

– Reynolds shear stress

$$R_{xz} = -\langle U'W' \rangle, \tag{12}$$

– resolved turbulent kinetic energy

$$K = \langle U'_i U'_i \rangle / 2, \tag{13}$$

– skewness of the mean streamwise velocity

$$S_u = \langle \bar{u}'^3 \rangle / \langle \bar{u}'^2 \rangle^{3/2}. \tag{14}$$

In order to assess the influence of the more comprehensive modelling we compare the current results to the previous study of [Schlegel et al. \(2012\)](#) who used a two-dimensional PAD. In the following, this case will be referred to as PAD-2D and the current one as PAD-3D. Finally, the field experiment is denoted as FIELD and the tower positions within the computational domain are given in Table 1.

4.2 Three-Dimensional Flow Characteristics

The superposition of the effects resulting, on the one hand, from the vegetation and, on the other hand, from the topography generates a complex flow structure throughout the solution domain. Herein we attempt to characterize the most prominent flow patterns occurring within the central region, since this is the main area of interest in the present study.

Figure 3 presents the iso-contours of the three mean velocity components within a vertical xz -plane at $Y = 0$. This position was chosen because it allows an intercomparison of the current results with the previous simulations of [Schlegel et al. \(2012\)](#) and visualizes the flow across the measurement transect. As expected, the mean streamwise velocity component decays quickly while passing the windward forest edge (luv) of the clearing. Further downstream U reaches values of about 0.2 inside the canopy. Noticeable is the deceleration of the flow at the upstream forest edge (lee). The mean streamwise velocity component approaches zero between $-7.5 \leq X \leq -6$, and seems to be related to a separation zone, located close to the ground within the wake zone of the edge. The flow reversal reaches a maximum velocity magnitude twice as large as in PAD-2D.

Table 2 presents the magnitudes of all velocity components within the central region. Notably, the cross-flow velocity component in PAD-3D is of the same order of magnitude as the vertical wind component. On the clearing this is closely linked to the inclined slope of the forest edge. Furthermore, the presence of the upstream hill and the depressed areas located

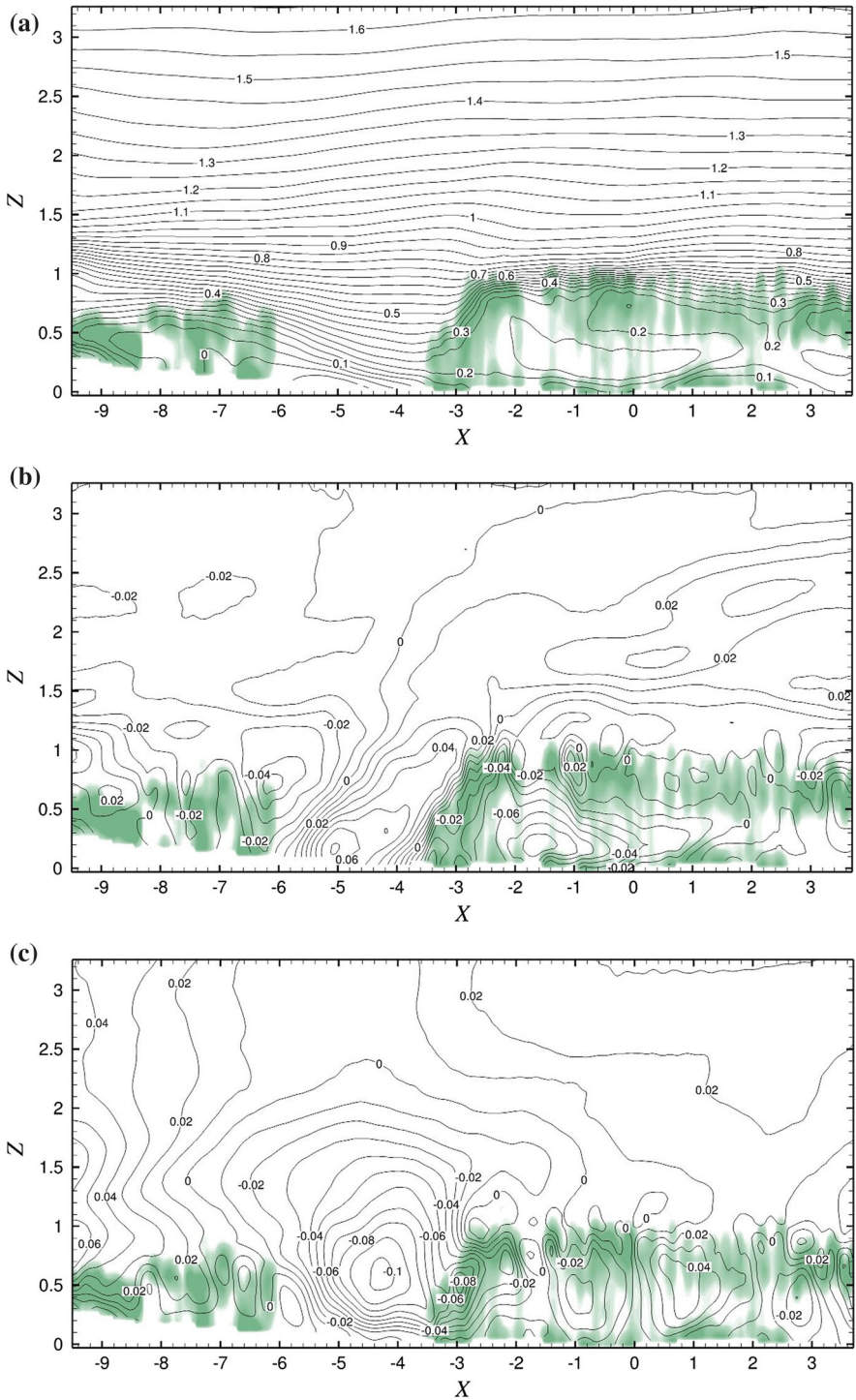


Fig. 3 Contours of the dimensionless mean velocity components for a vertical slice at $Y = 0$. The coordinates and values are normalized according to Eqs. 10 and 11. Colouring depicts the PAD values. **a** U , **b** V , **c** W

Table 2 Comparison of the normalized velocity magnitudes between PAD-2D and the central region of PAD-3D

| Simulation | U_{\min} | U_{\max} | V_{\min} | V_{\max} | W_{\min} | W_{\max} |
|------------|------------|------------|------------|------------|------------|------------|
| PAD-2D | -0.125 | 2.318 | -0.024 | 0.015 | -0.073 | 0.081 |
| PAD-3D | -0.213 | 2.398 | -0.229 | 0.293 | -0.131 | 0.078 |

The value for U_{\max} represents for both cases the normalized velocity magnitude at the upper boundary. Values are normalized according to Eq. 11

next to the lateral boundaries produce a cross-flow, too. Figure 3b indicates a significant positive lateral velocity component at the middle of the clearing, which changes its direction in the vicinity of the forest edges and vanishes inside the canopy. Despite the fact that Fig. 3b is a slice and not representative for the whole region, one may conclude that for real case scenarios the cross-flow velocity component has an influence on the horizontal momentum transport. This behaviour cannot be captured by a homogeneous or two-dimensional heterogeneous canopy description.

Figure 3c reveals a feature that is connected more to the small-scale plant heterogeneity: the mean vertical velocity component approaches its highest magnitude over the clearing, which extends over almost the complete height of the roughness sublayer. By this, fresh air from aloft is brought into the forest stand. It is also observable that the flow downstream of the forest edge does not attain an equilibrium state in terms of a vanishing vertical velocity component (Dupont and Brunet 2008a). Figure 3c indicates a noticeable upward and downward motion almost everywhere inside the canopy. This indicates that the vertical wind in the heterogeneous forest yields a considerable contribution to the energy and mass exchange within the atmospheric boundary layer.

To yield a measure for the distortion of the flow due to the presence of a clearing, the angle between the horizontal plane and the mean velocity vector at the location of the highest vertical wind speed in the vicinity of the windward forest edge was calculated for several xz -planes. It ranges between 11° and 23° along the edge, with a mean of about 17° , which is comparable to PAD-2D where we calculated 8° .

For a better impression of the flow field, the mean velocity vectors inside the vertical plane along the transect at $Y = 0$ are plotted in Fig. 4 and coloured with red, black and blue to mark the velocity component normal to the section plane. Following the flow downstream, we firstly identify an upward motion before reaching the upstream forest edge. The denser vegetation and the separation zone occurring in the wake of the edge forces the approaching flow to depart the canopy. At the windward end of the clearing the flow turns downward and penetrates the vegetation from aloft, which is in accordance with Frank and Ruck (2008). They observed that the flow across short clearings with a relative length of less than five times the tree height is dominated by the presence of a separation zone. The negative vertical velocity component persists till $X = -2$, and from thereon we observe an alternating upward and downward motion throughout the whole canopy. Figure 4 shows again the presence of a sustained lateral movement, especially across the clearing. At the leeward forest edge the colour of the velocity vectors indicates a negative, or southward, motion within the crown section and above, which is related to the edge shape. At the opposite end of the clearing the red colour suggests a positive, northward component of the flow. Again the shape of the forest edge is a possible explanation. Downstream inside the canopy the direction of the cross-flow velocity component turns towards negative values, which follows from continuity.

The presence of a significant lateral component of the velocity suggests a closer look into a horizontal xy -plane, e.g., $Z = 0.3$. Except in the vicinity of the clearing, where the tree

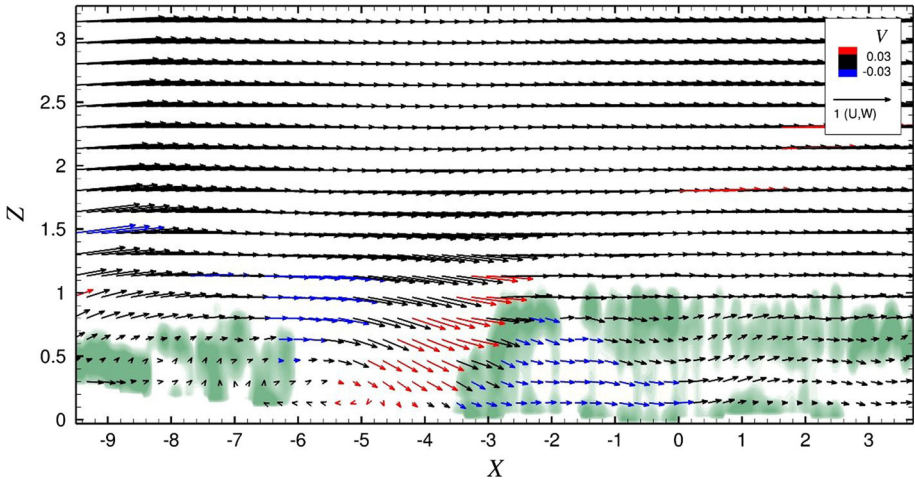


Fig. 4 Dimensionless mean velocity vector (U, V, W) in the plane $Y = 0$. Colouring of the vector depicts the lateral velocity component (V), with *red* indicating positive (northward) and *blue* negative (southward) motion. The coordinates and values are normalized according to Eqs. 10 and 11. The *empty area* in the *lower left corner* contains no data as it is located below the surface level. *Background colouring* depicts the *PAD* values

height and the crown-base height are lower than elsewhere, this plane represents mostly the part of the canopy below the tree crowns, the so-called trunk space. From the vector plot in Fig. 5a it is evident that the flow exposes a distinct three-dimensional character. Firstly, the velocity magnitude is small when compared to the reference velocity measured above the canopy. Nevertheless, a continuous change in the horizontal flow direction is observable all through the presented section of the solution domain. Associated with an upward and downward motion, this seems to be linked with the varying *PAD* and the topography. At the upstream boundary of the presented section the presence of the hill leads to a cross-flow velocity component in the negative y -direction (Fig. 2d). With the beginning at $X = -8$ the flow reacts on the locally denser vegetation and the influence of the clearing. The flow decelerates and changes continuously its direction. Finally, we observe a weak, edge-parallel flow at the upstream forest edge. A closer look reveals an associated upward and downward movement inside the forest stand and on the clearing, respectively. This is again an effect of the separation zone. To obtain an idea of its horizontal dimensions, Fig. 6 shows the projected contour of the zone characterized by a negative streamwise velocity component, covering a large part of the clearing and the surrounding forest stand. It is confined, however, to a height of $Z = 0.51$ and, thus, occurs only within the trunk space. The maximum backward velocity magnitude is reached at the southward corner of the clearing (Table 2).

The downstream part of the clearing (north-east) is not covered by the separation zone. Referring to Fig. 5a, the velocity vectors indicate three noticeable features within this region: firstly, an increase in velocity magnitude inside the horizontal plane; secondly, a downward motion. Both follow directly from continuity, as the flow has to fill the space due to the displacement of the flow reversal. Thirdly, we observe again a rotation of the wind direction. The flow seems to follow the edge until the end of the clearing. One might think that the flow attempts to avoid the denser vegetation and the associated higher aerodynamic resistance as long as possible. At the end of the clearing the flow passes the forest edge and traverses the trail path leaving our area of interest.

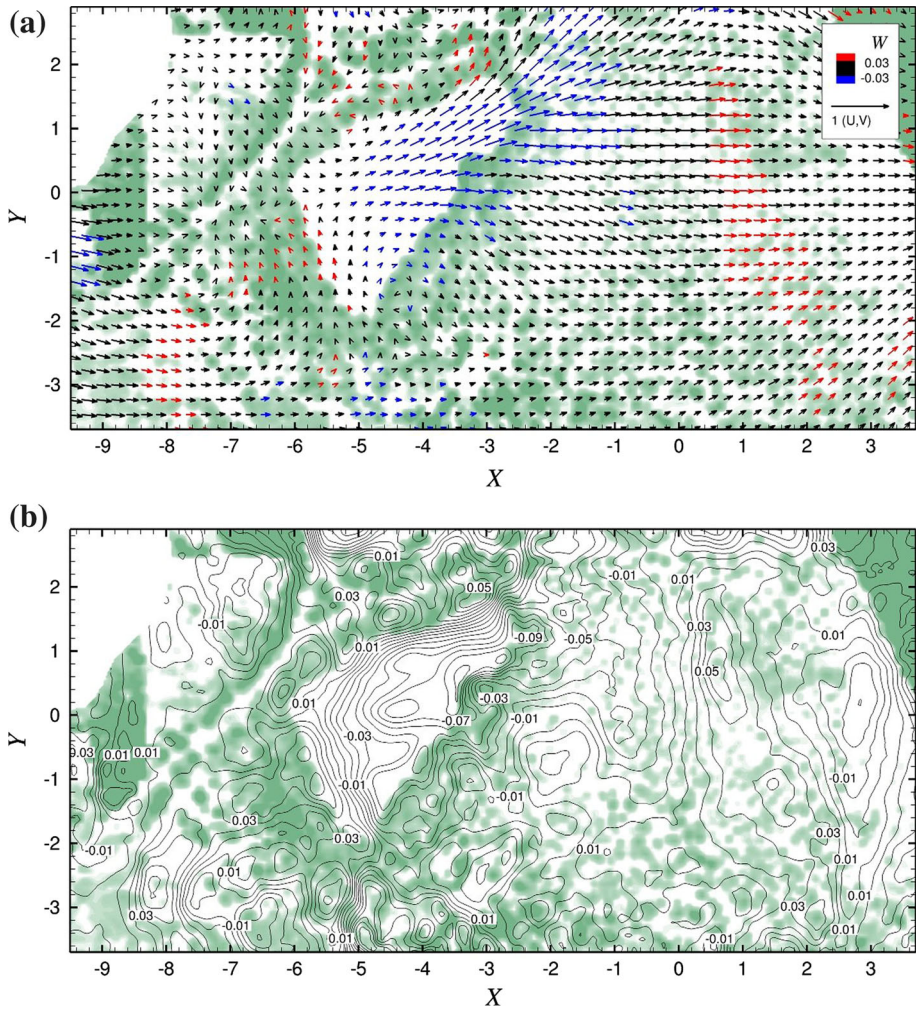


Fig. 5 Dimensionless projected mean velocity vector (U, V, W) and iso-contours of the mean vertical velocity component (W) for a horizontal slice at $Z = 0.3$. The coordinates and values are normalized according to Eq. 10 and 11. The empty area in the upper left corner contains no data since it is located below the surface level. Vector colouring depicts the vertical velocity component and background colouring the PAD values. **a** Dimensionless velocity vector (U, V, W). Colouring of the vector depicts the vertical velocity component (W), with colour coded upward (red) and downward (blue) motion, **b** W

From Fig. 5a we are able to identify further features that are closely linked to the distribution of the vegetation inside the trunk space. Upstream of the clearing, between $-8.5 \leq X \leq -7$ and $-3.6 \leq Y \leq -1.5$, we observe a field of positive vertical wind component. The PAI from Fig. 6 and the PAD reveal a sparse and low vegetation within this area. This, together with the local trail path, might lead to suction from the higher velocity air above the canopy. Another upwind field is visible downstream of the clearing between $0.5 \leq X \leq 2.5$ and $-3.6 \leq Y \leq 2$; the vertical velocity component varies around $W \approx 0.03$. Only within a smaller area between $0.4 \leq X \leq 0.8$ and $0.2 \leq Y \leq 1$, Fig. 5b shows a strong upwind flow velocity of larger than 5% of the reference velocity. A closer look to, e.g., Fig. 1

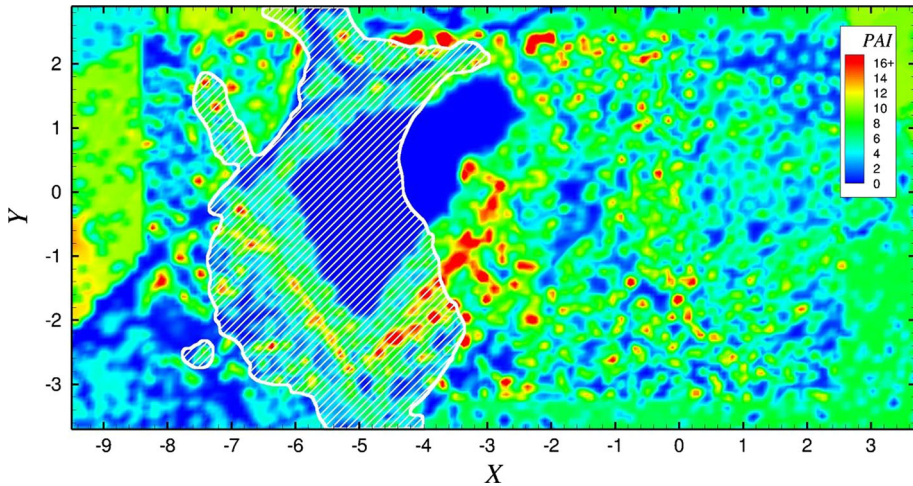


Fig. 6 Projected horizontal contours of the separation zone. Colouring depicts the *PAI* values with $2\text{ m} \times 2\text{ m}$ filter width

reveals again several larger tree gaps, which might be the reason for this behaviour. In this area, influences of the topography are visible as well. The mean flow heads more towards the middle of the domain, an effect of the depressed areas occurring at the lateral boundaries and the increasing terrain height towards the outflow boundary. Interestingly, the immediate influences from the vegetation and the topography vanish quickly above the nominal tree height ($Z > 1.0$). When looking at a horizontal plane at $Z = 1.3$ the flow is almost perfectly aligned to the mean flow direction (Figure not shown). Only a few fields of vertical wind velocity with a magnitude around $W = 0.03$ are visible. The most striking one appears above the clearing, where the downwind flow velocity still reaches 9 % of the reference velocity.

4.3 Comparison with Field Experiments

Figure 7 provides a comparison between computed and measured mean streamwise velocity at the position of the four measurement towers (see Table 1 for exact tower positions within the solution domain). Tower T1 stands close to the upwind edge of the clearing. Figure 7a shows a good agreement between PAD-3D and the measured mean velocity component U , whereas PAD-2D retains the typical S-shape of the velocity profile inside the canopy. This confirms the hypothesis of Schlegel et al. (2012) that an appropriate treatment of the upstream vegetation is crucial for capturing the conditions over the clearing. The agreement between PAD-3D and FIELD observations below $Z = 0.3$ is remarkable. Both measured and computed profiles reveal a backward oriented mean streamwise velocity component. The reason is the separation zone extending from the upstream canopy across the clearing. Within PAD-2D the separation zone was shifted towards the windward forest edge and, hence, tower T1 was located in front of it. Going upward, we first observe a good agreement for PAD-3D and FIELD data, turning into a slight overestimation for $Z \geq 0.6$. Above the canopy, within the roughness sublayer, the differences between both simulations vanish.

The following tower T2 is located immediately in front of the windward forest edge. Figure 7b confirms the trend observed at tower T1. Both simulations indicate a partial recovery of the logarithmic profile in the atmospheric surface layer and show a good qualitative agree-

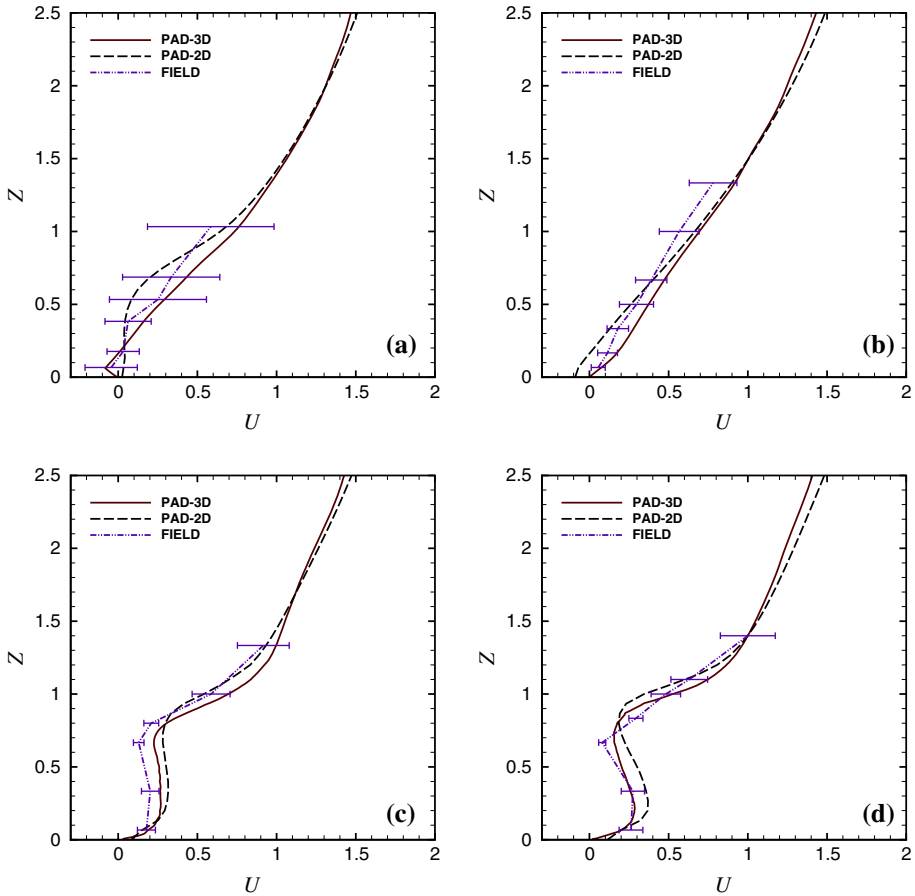


Fig. 7 Comparison of measured and computed normalized streamwise velocity profiles at the four measurement towers. The normalization is according to Eqs. 10 and 11. The tower positions are given in Fig. 1. **a** Tower T1, **b** Tower T2, **c** Tower T3, **d** Tower T4

ment with the experimental data. Nevertheless, PAD-3D is closer to FIELD data and benefits from the enhanced treatment of the vegetation and the topography. The occurrence of a separation zone within all numerical simulations, with a strong dependency on the employed *PAD* distribution arises some questions. Firstly, the proper treatment of the vegetation is crucial to obtain its correct position and dimension. Secondly, it suggests some further dependencies, e.g., thermal stratification, gusts or a shift in wind direction during the day that prevent a separation zone from being established and observed. Above the nominal tree height again both simulations converge to each other and, therefore, indicate less influence of the treatment of the vegetation underneath.

The next tower, T3, stands approximately two tree heights downstream of the windward forest edge. Both simulations and the field experiments show a rapid recovery of the S-shaped velocity profile. Despite the belt of chestnuts closing the trunk space at the forest edge, we observe also the first signs of the development of a secondary wind maximum below the crown section, which is quite common for tall forest stands with a sparse understorey (Shaw 1977). The qualitative agreement of the velocity profile between both simulations and FIELD

is satisfying, but especially in the trunk space, PAD-3D benefits from the enhanced treatment of the vegetation. Figure 7d presents the mean streamwise velocity component at the last tower T4. Here we observe an almost perfect match between PAD-3D and FIELD data with a well pronounced secondary wind maximum around $Z = 0.2$.

The exchange of momentum, heat and water vapour between a forest stand and the atmospheric boundary layer is mainly driven by the corresponding turbulent fluxes. Another contribution amplified by the small-scale plant heterogeneity arises from the mean vertical velocity component, which never vanishes completely as opposed to a homogeneous forest. During field experiments ultrasonic anemometers are the commonly used measurement devices. When used under non-ideal conditions, the ultrasonic anemometers show a considerable sensitivity with respect to the angle of attack and the wind direction (Kochendorfer et al. 2012). Additionally, the vertical velocity component is usually one order of magnitude less than the streamwise velocity component in magnitude, which makes levelling an important issue. Kochendorfer et al. (2012) conducted a reference experiment, where they compared different types of ultrasonic anemometer. Among others, the type used mainly in the presented field study, a Model 81000V (R.M. Young Meteorological Instruments, Michigan, USA), was tested for several angles of attack and wind directions. The authors determined an underestimation for the turbulent fluxes of about 10–15% when measured with a R.M. Young 81000V instrument.

Despite the discussion on the measurement of the vertical wind velocity component (Kochendorfer et al. 2012; Mauder 2013; Kochendorfer et al. 2013), we decided to compare our computed and observed results shown in Fig. 8 with respect to the previously mentioned uncertainties. When looking at the results for tower T1 in Fig. 8a, PAD-3D gives more reliable mean flow conditions on the clearing than PAD-2D. It reveals an upwards directed wind for $Z \leq 0.4$, turning towards a downwind above, corresponding nicely to the experimental data.

At the second tower on the clearing, T2, both simulations agree well with the experimental data, predicting a negative vertical wind component in front of the downstream forest edge. The maximum is reached around $Z = 0.7$, where it starts to decrease. Going further downstream into the canopy at tower T3 and T4 the magnitude of the vertical velocity component decreases as expected from the impact of drag forces (Fig. 8c, d). Both simulations stay almost within the measurement uncertainties, which are admittedly large. The vertical wind component ranges between $\pm 2\%$ of the reference velocity and PAD-3D reveals a slightly smaller magnitude than PAD-2D. Noticeable, and ‘an indication’ of the measuring difficulties, are the spikes within the crown section at both towers. Up to now there is no explanation and no counterpart in the numerical simulation for that. Above the nominal tree the behaviour changes when compared to both towers located on the clearing.

4.4 Statistics

The three-dimensionality of the *PAD* values also influences the turbulent quantities. To investigate this in more detail, Fig. 9 shows the normalized turbulent kinetic energy (TKE) K for the vertical slice at $Y = 0$ and the horizontal slice at $Z = 0.3$. Noteworthy is the enhancement of the turbulent fluctuations above the clearing that extends towards $Z = 1.8$. Starting at the upstream forest stand this region covers the whole clearing and ends in front of the windward forest edge. The highest magnitude is reached at $X \approx -5$ and $Z \approx 1.1$. When compared to the results of PAD-2D its location is shifted upstream as the shear layer between the separation zone and the outer flow. Further downstream the turbulence decays rapidly while passing the denser and largely closed edge. A similar behaviour is visible at the crown section since the main features of the local vegetation are the same. Inside the forest stand

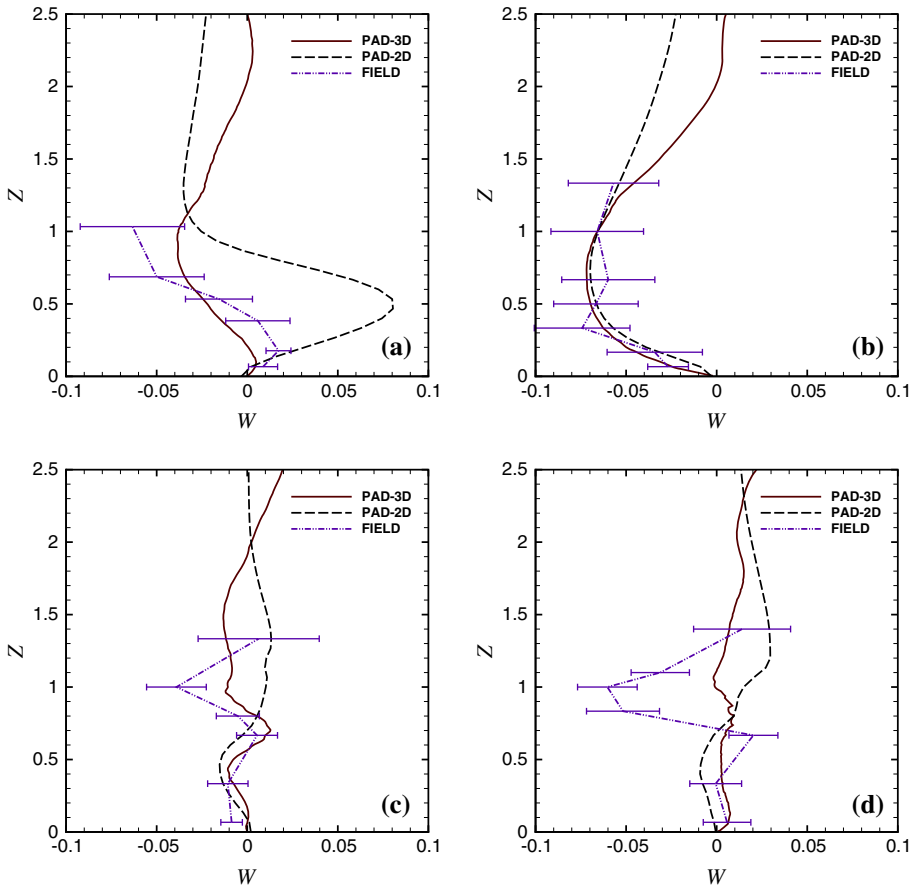


Fig. 8 Comparison of measured and computed normalized vertical velocity profiles at the four measurement towers. The normalization is according to Eqs. 10 and 11. The tower positions are given in Fig. 1. **a** Tower T1, **b** Tower T2, **c** Tower T3, **d** Tower T4

the TKE remains at values of $K \approx 0.01$ and no intrusion across the windward forest edge takes place. Therefore, K is one order of magnitude smaller than in the outer flow. Figure 9b confirms the low turbulent intensity within the whole forest stand except for the clearing and the first surrounding tree rows. The highest magnitude in the horizontal slice is reached in front of the windward edge and located between $-4.4 \leq X \leq -3.2$ and $-0.2 \leq Y \leq 0.8$. Referring to Fig. 5a, which shows the mean velocity vectors, this is exactly that part of the clearing where the flow starts to descend and accelerate. Together with the intermittent character of the separation zone (Raupach et al. 1987; Cassiani et al. 2008) this might explain the increase in K .

The Reynolds stress R_{xz} , characterizing the turbulent vertical momentum flux, behaves similarly to K . Figure 10 shows the contours for the selected slices. As with the TKE, R_{xz} is enhanced above the clearing as a result of the presence of the separation zone (Fig. 10a) and reaches its maximum slightly earlier at $X \approx -5.5$ and $Z \approx 1$. More striking is a secondary maximum further downstream between $0.2 \leq X \leq 2$ near the tree top. The intensity of the turbulent vertical momentum transport is here comparable to its values at the clearing. While

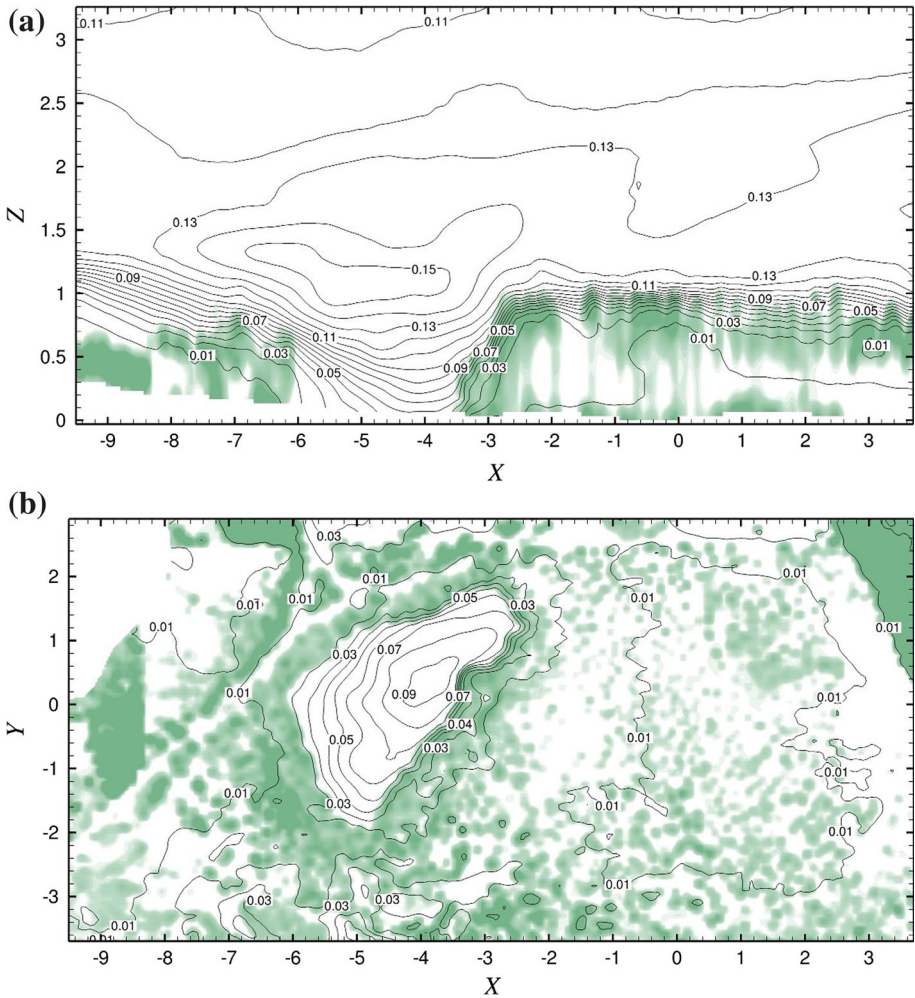


Fig. 9 Normalized turbulent kinetic energy K . The coordinates and values are normalized according to Eqs. 10 and 13. Colouring depicts the PAD values. **a** Vertical slice at $Y = 0$. **b** Horizontal slice at $Z = 0.3$

passing the denser and largely closed vegetation along the forest edge R_{xz} decreases rapidly and vanishes later in the trunk space throughout the whole forest stand (Fig. 10b). Actually, the sign of the turbulent momentum flux reverses, but with $R_{xz} \approx -0.004$ the magnitude is rather small. Higher values for R_{xz} are limited to the clearing and only a few areas elsewhere, e.g., between $-5.5 \leq X \leq -3.5$ and $-3.5 \leq Y \leq -2.5$ show noticeable exceptions.

An advantage of the snapshots from the instantaneous velocity field is the domain-wide access to higher-order statistics, e.g., the skewness of the velocity fluctuations in the mean flow direction S_u . This contains information on the distribution of the intensity and the size of the turbulent scales. Dupont and Brunet (2008a) used this quantity to identify an enhanced gust zone downstream of a forest edge, which is characterized by $S_u \geq 1.5$. Nevertheless, the pioneering work of Raupach et al. (1987) with a wind-tunnel experiment revealed an enhanced skewness of $S_u \geq 1.5$ within the crown section at $Z \approx 0.8$ about $5 h_{\text{ref}}$ downstream of the

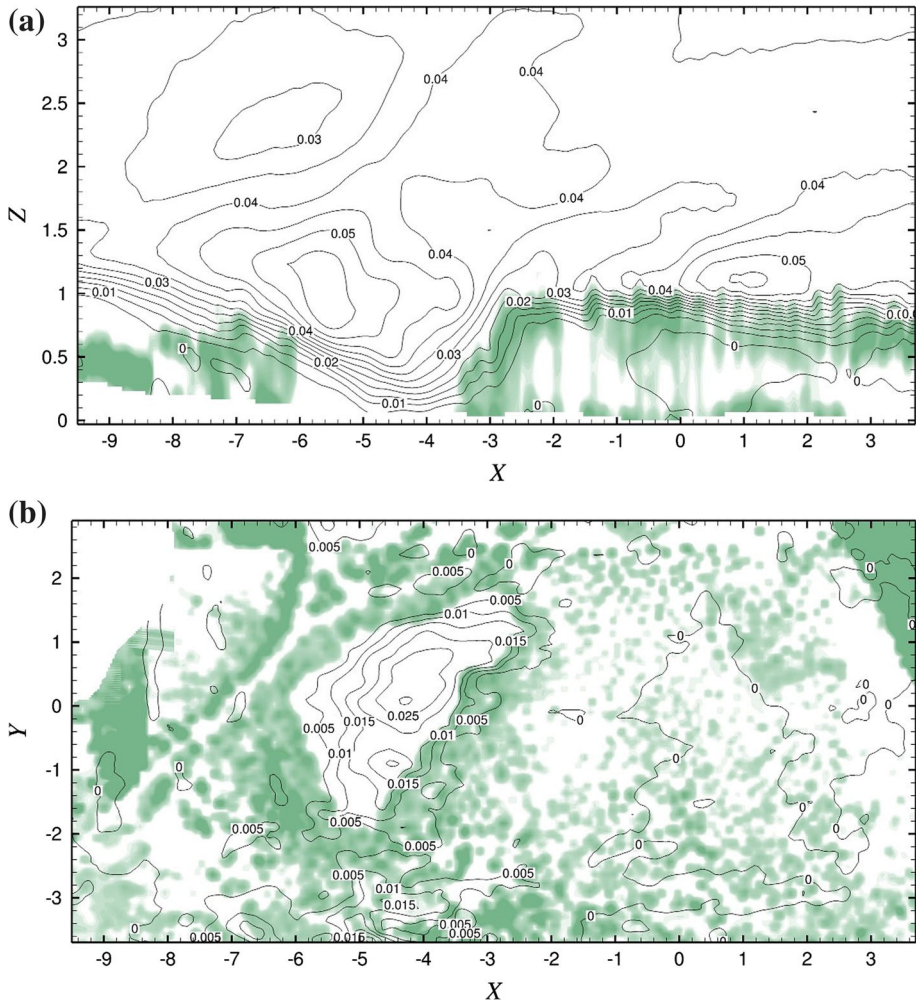


Fig. 10 Normalized Reynolds stress R_{xz} . The coordinates and values are normalized according to Eqs. 10 and 12. Colouring depicts the PAD values. **a** Vertical slice at $Y = 0$. **b** Horizontal slice at $Z = 0.3$

considered forest edge. Figure 11a shows S_u along the transect for the vertical slice at $Y = 0$, and clearly indicates an area characterized by a larger skewness downstream of the clearing between $0 \leq X \leq 2$ and $0.6 \leq Y \leq 1.0$. The highest magnitude of $S_u = 1.4$ is reached at $X = 0.7$ and $Z = 0.84$, which gives a relative length of about $4h_{ref}$ to the windward forest edge. To ensure that this is not a local phenomenon, Fig. 11b shows a horizontal slice at $Z = 0.8$, chosen according to the experimental results of Raupach et al. (1987). Two things are remarkable: first, an increased skewness occurs everywhere downstream of the windward forest edge. Secondly, the exact position (one to four times the tree height) and intensity ($0.8 \leq S_u \leq 1.4$) of the enhanced gust zone change. Qualitatively, our results match the predictions of Raupach et al. (1987) and Dupont and Brunet (2008a). However, both assumed ideal conditions in terms of a homogeneous forest, which explains the difference in magnitude of S_u . A comparison with the field experiment FIELD data shows that the value of

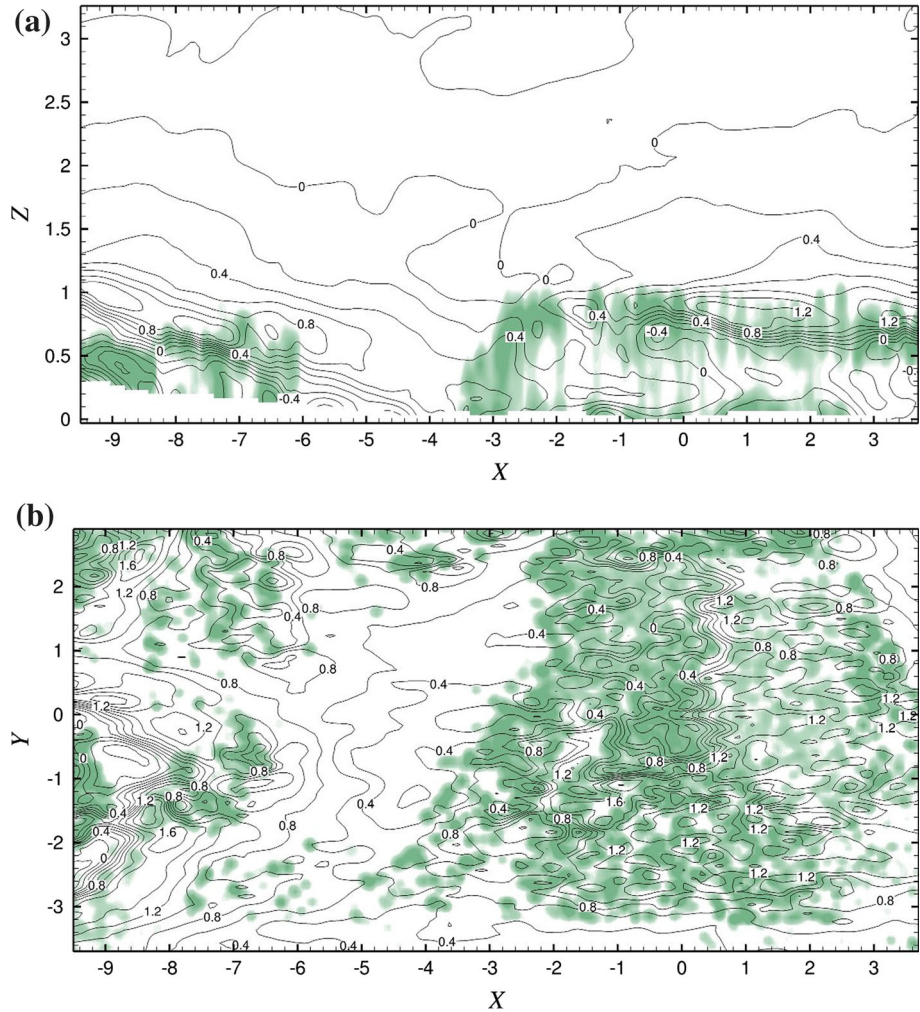


Fig. 11 Skewness of the mean streamwise velocity component fluctuations S_u . The coordinates are normalized according to Eqs. 10. Skewness is calculated from instantaneous snapshots following Eq. 14. Colouring depicts the PAD values. **a** Vertical slice at $Y = 0$. **b** Horizontal slice at $Z = 0.8$

$Z = 0.833$ for the maximum magnitude of S_u is predicted well by PAD-3D, and also fits the results of Raupach et al. (1987). But the computed magnitude of the skewness, $S_u = 0.77$, reaches only half of the measured value with $S_u = 1.49$. This might be explained by a closer inspection of Fig. 11a. In PAD-3D the main tower is located in front of the enhanced gust zone, and a shift downstream of a few m, would improve the agreement with FIELD observations. Nevertheless, the computed skewness fits well to the measurements.

Finally, Figs. 12, 13 and 14 provide a comparison of the computed and measured turbulent quantities at the four measurement towers. Overall, the TKE fits well with the field experiment (Fig. 12). Inside the forest stand K stays below 0.02 and higher values are reached only within the shear layer above the canopy and across the clearing. Thus, at the latter, the biggest differences are formed between both numerical simulations. As the conditions there

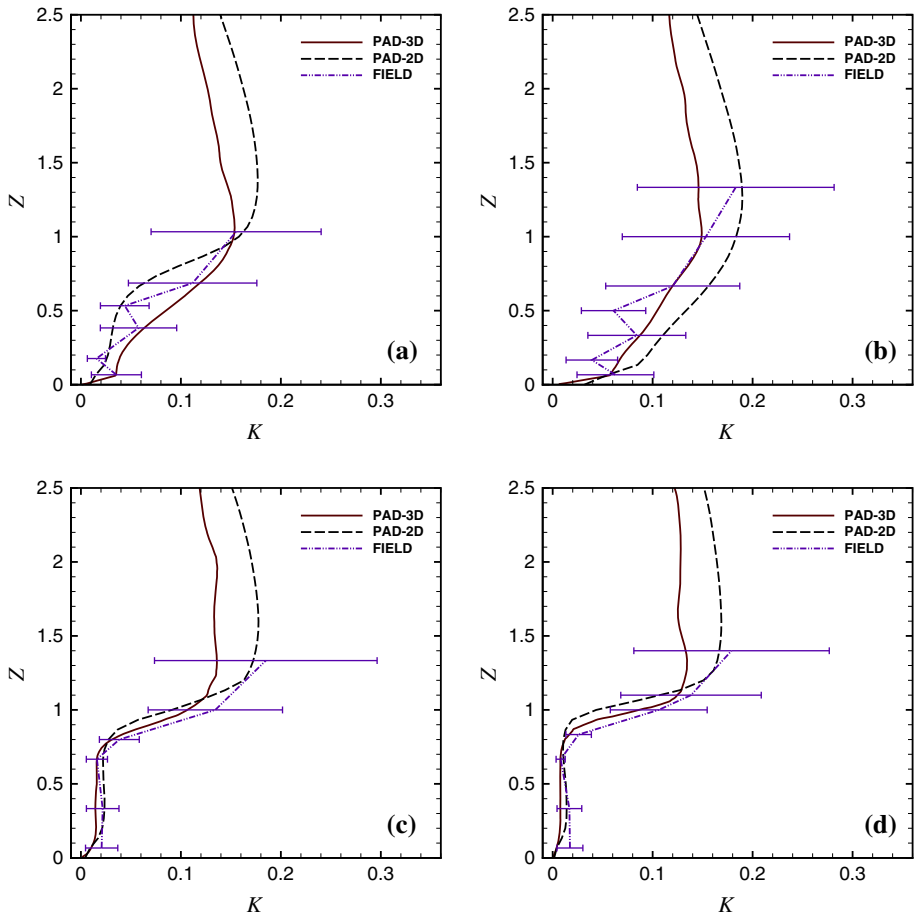


Fig. 12 Comparison of measured and computed profiles for normalized turbulent kinetic energy K at the four measurement towers. The normalization is according to Eqs. 10 and 13. The tower positions are given in Fig. 1. **a** Tower T1, **b** Tower T2, **c** Tower T3, **d** Tower T4

are mainly influenced by the separation zone, PAD-3D shows a better agreement with FIELD data than PAD-2D. The highest magnitude of K at all towers is reached inside the shear layer above the canopy. But again, the field measurements are extremely sensitive to the filtering of the raw data and the statistical uncertainty is high.

The advantage of a three-dimensional small-scale plant heterogeneity is more obvious for the Reynold stress R_{xz} and, in particular, for the towers located on the clearing (Fig. 13). Especially tower T1 shows for PAD-3D not only a quantitative, but also a qualitative, improvement and at tower T2 the overestimation of R_{xz} is much less compared to PAD-2D. Further downstream inside the forest stand the differences between both numerical simulations vanish, which might be caused by the low order of magnitude of R_{xz} . At tower T4 we observe a small counter-gradient momentum flux. Thus, the differences between both simulations and the field measurements at tower T3 and T4 remain negligible for $Z \leq 0.7$. At this height, R_{xz} starts to increase and reaches its highest magnitude inside the shear layer above the canopy as with K before. Further upward, leaving the shear layer, R_{xz} decreases

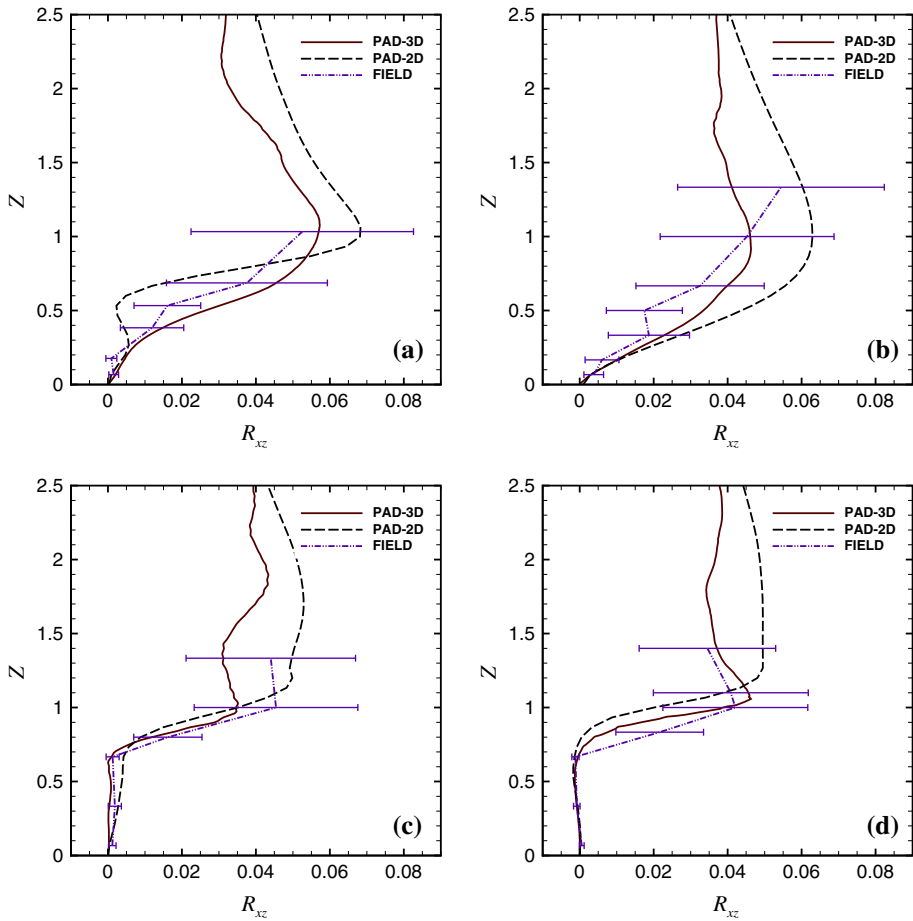


Fig. 13 Comparison of measured and computed profiles for normalized Reynolds stress R_{xz} at the four measurement towers. The normalization is according to Eqs. 10 and 12. The tower positions are given in Fig. 1. **a** Tower T1, **b** Tower T2, **c** Tower T3, **d** Tower T4

as a result of the artificial boundary conditions at the top of the domain. PAD-2D shows the expected behaviour, whereas it is delayed in PAD-3D and R_{xz} remains constant until $Z = 1.5 \dots 2$. This suggests a sufficient choice of the height of the solution domain, since a constant turbulent vertical momentum flux is typical for this part of the atmospheric boundary layer (Eting 2008; Kraus 2008; Fernando 2012a, b).

Within the three-dimensional forest environment in PAD-3D, another component of the Reynolds-stress tensor might cause a vertical momentum transport by turbulent motions. Figure 14 shows R_{yz} at the positions of the four measurement towers. Inside the forest stand below $Z \leq 0.7$ R_{yz} shows similarly low values as R_{xz} . However, at locations where R_{xz} causes a significant vertical transport of momentum, e.g., the crown section and the clearing, R_{yz} stays below 0.005 and never exceeds 0.01, whereas R_{xz} assumes values between 0.04 and 0.08. Despite the three-dimensionality of the vegetation, the turbulent transport of momentum is still mainly driven by R_{xz} . PAD-3D and the field measurements agree qualitatively and quantitatively well, but the exception to the rule is tower T3. For $Z \geq 0.7$ PAD-3D and

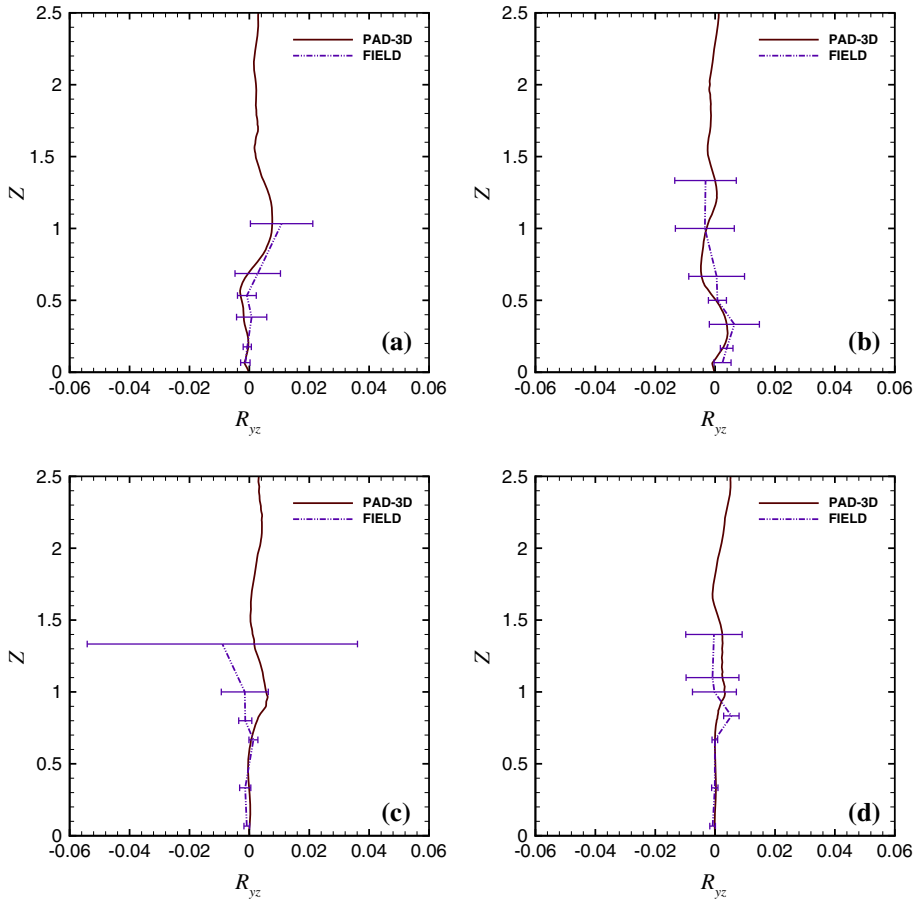


Fig. 14 Comparison of measured and computed profiles for normalized Reynolds stress R_{yz} at the four measurement towers. The normalization is according to Eqs. 10 and 12. The tower positions are given in Fig. 1. **a** Tower T1, **b** Tower T2, **c** Tower T3, **d** Tower T4

FIELD data show larger differences and finally the turbulent momentum flux represented by R_{yz} has an opposite sign. However, the measurement uncertainty at this point is extremely high and one should add less authority to it.

5 Conclusion

The canopy flow through a fully three-dimensional forest stand was investigated by means of LES, and an aerodynamic resistance was used to model the influence of the vegetation on the turbulent flow. The virtual forest, more precisely *PAD* values were obtained by terrestrial laser scanning for one sixth of the computational domain. For the first time, the vegetation within a numerical simulation was characterized by a three-dimensional small-scale plant heterogeneity representing a real canopy. The remaining domain was filled with the virtual canopy generator of Bohrer et al. (2007) based on forest inventory maps and airborne laser

scanning data. In combination, both distributions yielded a domain-wide three-dimensional heterogeneous *PAD* for the numerical simulation. As an additional feature the topography was included in terms of a modified digital terrain model.

The turbulent flow through the canopy shows a considerable complexity due to the interaction of topography and plant heterogeneity. Near the clearing we observe a distinct three-dimensional flow structure, which is characterized by an extended separation zone in the upstream region and a strong cross-flow along the oblique windward edge. In addition to this, small-scale plant heterogeneity leads to a corresponding pattern of sustained upward and downward motions, which were already reported in Schlegel et al. (2012). This vertical wind component induces an additional momentum transport throughout the canopy, which could not be captured by using a homogeneous *PAD*. For the turbulent quantities, the present study confirms that the dense windward forest edge efficiently dissipates the fluctuations within the incoming flow. As a new feature, local minima and maxima for the Reynolds stress component R_{xz} were observed that have no counterpart in the turbulent kinetic energy. Furthermore, we were able to detect an enhanced gust zone downstream of the windward forest edge. The comparison between the numerical simulations and the field measurements shows excellent agreement for the mean flow as well as for turbulent statistics.

In summary, we conclude that the inclusion of a high resolution plant representation combined with a digital terrain model allows for a more accurate prediction of the turbulent flow through heterogeneous canopies. Future work should be focused on a deeper understanding of the distinct effects of heterogeneity.

Acknowledgments The work was supported by the German National Science Foundation (Deutsche Forschungsgemeinschaft, DFG) within the project “Turbulent Exchange Processes between Forested Areas and the Atmosphere” as a part of the DFG priority programme 1276 MetStröm: Multiple Scales in Fluid Mechanics and Meteorology. Computational facilities were provided by the Center for Information Services and High Performance Computing (ZIH) of the Technische Universität Dresden. We gratefully acknowledge Gil Bohrer at the Ohio State University, USA for his comments and his help on the adaptation of the virtual canopy generator. We also thank the two anonymous reviewers whose comments significantly improved the quality of the article.

References

- Aschoff T, Spiecker H (2004) Algorithms for the automatic detection of trees in laser scanner data. In: International archives of the photogrammetry, remote sensing and spatial information sciences, vol 36, part 8/W2, pp 71–75
- Bailey B, Stoll R (2013) Turbulence in sparse, organized vegetative canopies: a large-eddy simulation study. *Boundary-Layer Meteorol* 147:369–400
- Belcher S, Finnigan J, Harman I (2008) Flows through forest canopies in complex terrain. *Ecol Appl* 18(6):1436–1453
- Belcher S, Harman I, Finnigan J (2012) The wind in the willows: flows in forest canopies in complex terrain. *Annu Rev Fluid Mech* 44:479–504
- Bernhofer C, Aubinet M, Clement R, Grelle A, Grünwald T, Ibrom A, Jarvis P, Rebmann C, Schulze E, Tenhunen J (2003) Fluxes of carbon, water and energy of European Forests, vol 163 of Ecological studies, chap. Spruce forests (Norway and Sitka spruce, including Douglas fir): carbon and water fluxes and balances, ecological and ecophysiological determinants. Springer, Berlin, pp 99–123, 273 pp
- Bienert A, Maas H-G (2009) Methods for the automatic geometric registration of terrestrial laserscanner point clouds in forest stands. In: International archives of the photogrammetry, remote sensing and spatial information sciences, vol 38, part 3/W8, pp 1–6
- Bienert A, Queck R, Schmidt A, Bernhofer C, Maas H-G (2010) Voxel space analysis of terrestrial laser scans in forests for wind field modelling. In: International archives of the photogrammetry, remote sensing and spatial information sciences, vol 38, part 5, pp 92–97

- Bienert A, Pech K, Maas H-G (2011) Verfahren zur Registrierung von Laserscannerdaten in Waldbeständen. *Swiss For J* 162:178–185
- Bohrer G, Wolosin M, Brady R, Avissar R (2007) A virtual canopy generator (V-CaGe) for modelling complex heterogeneous forest canopies at high resolution. *Tellus B* 59:566–576
- Bohrer G, Katul G, Nathan R, Walko R, Avissar R (2008) Effects of canopy heterogeneity, seed abscission and inertia on wind-driven dispersal kernels of tree seeds. *J Ecol* 96:569–580
- Bohrer G, Katul G, Walko R, Avissar R (2009) Exploring the effects of microscale structural heterogeneity of forest canopies using large-eddy simulations. *Boundary-Layer Meteorol* 132:351–382
- Brunet Y, Irvine M (2000) The control of coherent eddies in vegetation canopies: streamwise structure spacing, canopy shear scale and atmospheric stability. *Boundary-Layer Meteorol* 94:139–163
- Bundesministerium für Ernährung, Landwirtschaft und Verbraucherschutz (2009) *Waldbericht der Bundesregierung 2009*, 117 pp
- Cassiani M, Katul G, Albertson J (2008) The effects of canopy leaf area index on airflow across forest edges: large-eddy simulation and analytical results. *Boundary-Layer Meteorol* 126:433–460
- Chen J, Black T (1991) Measuring leaf area index of plant canopies with branch architecture. *Agric For Meteorol* 57:1–12
- Chester S, Meneveau C (2007) Renormalized numerical simulation of flow over planar and non-planar fractal trees. *Environ Fluid Mech* 7:289–301
- Dalpe B, Masson C (2009) Numerical simulation of wind flow near a forest edge. *J Wind Eng Ind Aerodyn* 97:228–241
- de Langre E (2008) Effects of wind on plants. *Annu Rev Fluid Mech* 40:141–168
- Deardorff J (1980) Stratocumulus-capped mixed layers derived from a three-dimensional model. *Boundary-Layer Meteorol* 18:495–527
- Detto M, Katul G, Siqueira M, Juang J-Y, Stoy P (2008) The structure of turbulence near a tall forest edge: the backward-facing step flow analogy revisited. *Ecol Appl* 18:1420–1435
- Dupont S, Brunet Y (2006) Simulation of turbulent flow in an urban forested park damaged by a windstorm. *Boundary-Layer Meteorol* 120:133–161
- Dupont S, Brunet Y (2008a) Edge flow and canopy structure: a large-eddy simulation study. *Boundary-Layer Meteorol* 126:51–71
- Dupont S, Brunet Y (2008b) Impact of forest edge shape on tree stability: a large-eddy simulation study. *Forestry* 81:299–315
- Dupont S, Brunet Y (2008c) Influence of foliar density profile on canopy flow: a large-eddy simulation study. *Agric For Meteorol* 148:976–990
- Dupont S, Brunet Y (2009) Coherent structures in canopy edge flow: a large-eddy simulation study. *J Fluid Mech* 630:93–128
- Dupont S, Brunet Y, Finnigan JJ (2008) Large-eddy simulation of turbulent flow over a forested hill: validation and coherent structure identification. *Q J R Meteorol Soc* 134:1911–1929
- Dupont S, Bonnefond J-M, Irvine M, Lamaud E, Brunet Y (2011) Long-distance edge effects in a pine forest with a deep and sparse trunk space: in situ and numerical experiments. *Agric For Meteorol* 151:328–344
- Dupont S, Irvine M, Bonnefond J-M, Lamaud E, Brunet Y (2012) Turbulent structures in a pine forest with a deep and sparse trunk space: stand and edge regions. *Boundary-Layer Meteorol* 143:309–336
- Edburg S, Stock D, Lamb B, Patton E (2012) The effect of the vertical source distribution on scalar statistics within and above a forest canopy. *Boundary-Layer Meteorol* 142:365–382
- Eder F, Serafimovich A, Foken T (2013) Coherent structures at a forest edge: properties, coupling and impact of secondary circulations. *Boundary-Layer Meteorol* 148:285–308
- Endalew A, Hertog M, Delele M, Baelmans M, Ramon H, Nicolai B, Verboven P (2009) CFD modelling of turbulent airflow through plant systems using 3D canopy architecture. In: *Turbulent Heat Mass Transfer* 6, 12 pp
- Endalew A, Debaer C, Rutten N, Vercammen J, Delele M, Ramon H, Nicolai B, Verboven P (2011) Modelling the effect of tree foliage on sprayer airflow in orchards. *Boundary-Layer Meteorol* 138:139–162
- Etiling D (2008) *Theoretische Meteorologie: Eine Einführung*, vol 3. Springer, Berlin 388 pp
- Feigenwinter C, Bernhofer C, Vogt R (2004) The influence of advection on the short term CO₂-budget in and above a forest canopy. *Boundary-Layer Meteorol* 113:201–224
- Fernando H (ed) (2012a) *Handbook of environmental fluid dynamics*, vol 1: overview and fundamentals. CRC Press, Boca Raton, 635 pp
- Fernando H (ed) (2012b) *Handbook of environmental fluid dynamics*, vol 2: systems, pollution, modeling, and measurements. CRC Press, Boca Raton, 587 pp
- Fesquet C, Dupont S, Drobinski P, Dubos T, Barthlott C (2009) Impact of terrain heterogeneity on coherent structure properties: numerical approach. *Boundary-Layer Meteorol* 133:71–92
- Finnigan J (2000) Turbulence in plant canopies. *Annu Rev Fluid Mech* 32:519–571

- Finnigan J, Belcher S (2004) Flow over a hill covered with a plant canopy. *Q J R Meteorol Soc* 130:1–29
- Finnigan J, Brunet Y (1995) Wind and trees, chap Turbulent airflow in forests on flat and hilly terrain. Cambridge University Press, Cambridge, pp 3–40, 504 pp
- Finnigan J, Shaw R, Patton E (2009) Turbulence structure above a vegetation canopy. *J Fluid Mech* 637:387–424
- Fitzmaurice L, Shaw R, Paw UK, Patton E (2004) Three-dimensional scalar microfront systems in a large-eddy simulation of vegetation canopy flow. *Boundary-Layer Meteorol* 112:107–127
- Fontan S, Katul G, Poggi D, Manes C, Ridolfi L (2013) Flume experiments on turbulent flows across gaps of permeable and impermeable boundaries. *Boundary-Layer Meteorol* 147:21–39
- Frank C, Ruck B (2008) Numerical study of the airflow over forest clearings. *Forestry* 81:259–277
- Gao W, Shaw R, Paw U K (1989) Observation of organized structure in turbulent flow within and above a forest canopy. *Boundary-Layer Meteorol* 47:349–377
- Gavrilov K, Accary G, Morvan D, Lyubimov D, Mradji S, Bessonov O (2011) Numerical simulation of coherent structures over plant canopy. *Flow Turbul Combust* 86:89–111
- Graham J, Meneveau C (2012) Modeling turbulent flow over fractal trees using renormalized numerical simulation: alternate formulations and numerical experiments. *Phys Fluids* 24:1–32
- Grünwald T, Bernhofer C (2007) A decade of carbon, water and energy flux measurements of an old spruce forest at the Anchor Station Tharandt. *Tellus B* 59:387–396
- Harman I, Finnigan J (2010) Flow over hills covered by a plant canopy: extension to generalised two-dimensional topography. *Boundary-Layer Meteorol* 135:51–65
- Harman I, Finnigan J (2013) Flow over a narrow ridge covered with a plant canopy: a comparison between wind-tunnel observations and linear theory. *Boundary-Layer Meteorol* 147:1–20
- Huang J, Katul G, Albertson J (2013) The role of coherent turbulent structures in explaining scalar dissimilarity within the canopy sublayer. *Environ Fluid Mech* 13:571–599
- Inoue E (1955) Studies of the phenomena of Waving plants (“HONAMI”) caused by wind. *J Agric Meteorol* 11:18–22
- Irvine M, Gardiner B, Hill M (1997) The evolution of turbulence across a forest edge. *Boundary-Layer Meteorol* 84:467–496
- Iwata H, Asanuma J, Qhtani Y, Mizoguchi Y, Yasuda Y (2009) Vertical length scale of transporting eddies for sensible heat in the unstable roughness sublayer over a forest canopy. *J Agric Meteorol* 65:1–9
- Jasak H (1996) Error analysis and estimation for the finite volume method with applications to fluid flows. PhD Thesis, Imperial College, London
- Juang J-Y, Katul G, Siqueira M, Stoy P, McCarthy H (2008) Investigating a hierarchy of Eulerian closure models for scalar transfer inside forested canopies. *Boundary-Layer Meteorol* 128:1–32
- Júnior C, Sá L, Pachêco V, de Souza C (2013) Coherent structures detected in the unstable atmospheric surface layer above the Amazon forest. *J Wind Eng Ind Aerodyn* 115:1–8
- Kaimal J, Finnigan J (1994) Atmospheric boundary layer flows. Oxford University Press, New York, 304 pp
- Katul G, Mahrt L, Poggi D, Sanz C (2004) One- and two-equation models for canopy turbulence. *Boundary-Layer Meteorol* 113:81–109
- Katul G, Finnigan J, Poggi D, Leuning R, Belcher S (2006) The influence of hilly terrain on canopy-atmosphere carbon dioxide exchange. *Boundary-Layer Meteorol* 118:189–216
- Kochendorfer J, Paw U K (2011) Field estimates of scalar advection across a canopy edge. *Agric For Meteorol* 151:584–594
- Kochendorfer J, Meyers T, Frank J, Massman W, Heuer M (2012) How well can we measure the vertical wind speed? Implications for fluxes of energy and mass. *Boundary-Layer Meteorol* 145:383–393
- Kochendorfer J, Meyers T, Frank J, Massman W, Heuer M (2013) Reply to the comment by Mauder on “How well can we measure the vertical wind speed? Implications for fluxes of energy and mass”. *Boundary-Layer Meteorol* 147:337–345
- Kraus H (2008) Grundlagen der Grenzschicht-Meteorologie. Springer, Berlin 214 pp
- Lee X (2000) Air motion within and above forest vegetation in non-ideal conditions. *For Ecol Manag* 135:3–18
- Lilly D (1967) The representation of small-scale turbulence in numerical simulation experiments. In: Proceedings of IBM scientific computing symposium environmental science, pp 1–24
- Lopes AS, Palma J, Lopes JV (2013) Improving a two-equation turbulence model for canopy flows using large-eddy simulation. *Boundary-Layer Meteorol* 149:231–257
- Lumley L, Panofsky H (1964) The structure of atmospheric turbulence. Interscience, New York, 239 pp
- Maas H-G, Bienert A, Scheller S, Keane E (2008) Automatic forest inventory parameter determination from terrestrial laserscanner data. *Int J Remote Sens* 29(5):1579–1593
- Mauder M (2013) A comment on “How well can we measure the vertical wind speed? Implications for fluxes of energy and mass” by Kochendorfer et al. *Boundary-Layer Meteorol* 147:329–335

- Monin S, Obukhov A (1954) Basic laws of turbulent mixing in the atmosphere near the ground. *Tr Acad Nauka SSR* 24:1963–1987
- Morse A, Gardiner B, Marshall B (2002) Mechanisms controlling turbulence development across a forest edge. *Boundary-Layer Meteorol* 103:227–251
- Novak M, Warland J, Orchansky A, Kettler R, Green S (2000) Wind tunnel and field measurements of turbulent flow in forests. Part I: uniformly thinned stands. *Boundary-Layer Meteorol* 95:457–495
- Orlanski I (1976) A simple boundary condition for unbounded hyperbolic flows. *J Comput Phys* 21:251–269
- Panferov O, Sogachev A (2008) Influence of gap size on wind damage variables in a forest. *Agric For Meteorol* 148:1869–1881
- Patton E, Finnigan J (2012) Handbook of environmental fluid dynamics, vol 1: overview and fundamentals, chap: Canopy turbulence. CRC Press, Boca Raton, pp 311–327, 635 pp
- Patton E, Katul G (2009) Turbulent pressure and velocity perturbations induced by gentle hills covered with sparse and dense canopies. *Boundary-Layer Meteorol* 133:189–217
- Patton E, Horst T, Sullivan P, Lenschow D, Oncley S, Brown W, Burns S, Guenther A, Held A, Karl T, Mayor S, Rizzo L, Spuler S, Sun J, Turnipseed A, Allwine E, Edburg S, Lamb B, Avissar R, Calhoun R, Kleissl J, Massman W, U K, Weil J (2011) The canopy horizontal array turbulence study. *Bull Am Meteorol Soc* 92:593–611
- Peters K, Eiden R (1992) Modelling the dry deposition velocity of aerosol particles to a spruce forest. *Atmos Environ* 26A:2555–2564
- Poggi D, Katul G (2007a) The ejection-sweep cycle over bare and forested gentle hills: a laboratory experiment. *Boundary-Layer Meteorol* 122:493–515
- Poggi D, Katul G (2007b) An experimental investigation of the mean momentum budget inside dense canopies on narrow gentle hilly terrain. *Agric For Meteorol* 144:1–13
- Poggi D, Katul G (2007c) Turbulent flows on forested hilly terrain: the recirculation region. *Q J R Meteorol Soc* 133:1027–1039
- Poggi D, Katul G, Albertson J, Ridolfi L (2007) An experimental investigation of turbulent flows over a hilly surface. *Phys Fluids* 19:1–12
- Poggi D, Katul G, Finnigan J, Belcher S (2008) Analytical models for the mean flow inside dense canopies on gentle hilly terrain. *Q J R Meteorol Soc* 134:1095–1112
- Poggi D, Katul G, Vidakovic B (2011) The role of wake production on the scaling laws of scalar concentration fluctuation spectra inside dense canopies. *Boundary-Layer Meteorol* 139:83–95
- Pope SB (2000) *Turbulent flows*. Cambridge University Press, Cambridge, UK, 806 pp
- Queck R, Bernhofer C (2010) Constructing wind profiles in forests from limited measurements of wind and vegetation structure. *Agric For Meteorol* 150:724–735
- Queck R, Bienert A, Maas H-G, Harmansa S, Goldberg V, Bernhofer C (2012) Wind fields in heterogeneous conifer canopies: parameterisation of momentum absorption using high-resolution 3D vegetation scans. *Eur J For Res* 131:165–176
- Raupach M, Thom A (1981) Turbulence in and above plant canopies. *Annu Rev Fluid Mech* 13:97–129
- Raupach M, Bradley E, Ghadiri H (1987) A wind tunnel investigation into the aerodynamic effect of forest clearings on the nesting of Abbott's Booby on Christmas Island. Tech Rep. CSIRO Div Environ Mech, Canberra, 23 pp
- Raupach M, Finnigan J, Brunet Y (1996) Coherent eddies and turbulence in vegetation canopies: the mixing-layer analogy. *Boundary-Layer Meteorol* 78:351–382
- Raynor G (1971) Wind and temperature structure in a coniferous forest and a contiguous field. *For Sci* 17:351–363
- Ross A (2008) Large-eddy simulations of flow over forested ridges. *Boundary-Layer Meteorol* 128:59–76
- Ross A (2011) Scalar transport over forested hills. *Boundary-Layer Meteorol* 141:179–199
- Ross A (2012) Boundary-layer flow within and above a forest canopy of variable density. *Q J R Meteorol Soc* 138:1259–1272
- Ross A, Baker T (2013) Flow over partially forested ridges. *Boundary-Layer Meteorol* 146:375–392
- Ross A, Vosper S (2005) Neutral turbulent flow over forested hills. *Q J R Meteorol Soc* 131:1841–1862
- Ruck B, Frank C, Tischmacher M (2012) On the influence of windward edge structure and stand density on the flow characteristics at forest edges. *Eur J For Res* 131:177–189
- Sagaut P (1998) *Large eddy simulation for incompressible flows*. Springer, Berlin 426 pp
- Schlegel F, Stiller J, Bienert A, Maas H-G, Queck R, Bernhofer C (2012) Large-eddy simulation of inhomogeneous canopy flows using high resolution terrestrial laser scanning data. *Boundary-Layer Meteorol* 142:223–243
- Schlichting H, Gersten K (2000) *Boundary layer theory*, 8th edn. Springer, Berlin
- Schmidt H, Schumann U (1989) Coherent structure of the convective boundary layer derived from large-eddy simulations. *J Fluid Mech* 200:511–562

- Schrötte J, Dörnbrack A (2013) Turbulence structure in a diabatically heated forest canopy composed of fractal Pythagoras trees. *Theor Comput Fluid Dyn* 23:337–359
- Serafimovich A, Thomas C, Foken T (2011) Vertical and horizontal transport of energy and matter by coherent motions in a tall spruce canopy. *Boundary-Layer Meteorol* 140:429–451
- Shaw R (1977) Secondary wind speed maxima inside plant canopies. *J Appl Meteorol* 16:514–521
- Shaw R, Patton E (2003) Canopy element influences on resolved- and subgrid-scale energy within a large-eddy simulation. *Agric For Meteorol* 115:5–17
- Shaw R, Pereira A (1982) Aerodynamic roughness of a plant canopy: a numerical experiment. *Agric Meteorol* 26:51–65
- Shaw R, Schumann U (1992) Large-eddy simulation of turbulent flow above and within a forest. *Boundary-Layer Meteorol* 61:47–64
- Shaw R, den Hartog G, Neumann H (1988) Influence of foliar density and thermal stability on profiles of Reynolds stress and turbulence intensity in a deciduous forest. *Boundary-Layer Meteorol* 45:391–409
- Sogachev A (2009) A note on two-equation closure modelling of canopy flow. *Boundary-Layer Meteorol* 130:423–435
- Sogachev A, Leclerc M, Zhang G, Rannik U, Vesala T (2008) CO₂ fluxes near a forest edge: a numerical study. *Ecol Appl* 16(6):1454–1469
- Sogachev A, Panferov O, Ahrends B, Doering C, Jørgensen H (2011) Numerical assessment of the effect of forest structure changes on CO₂ flux footprints for the flux tower in Solling, Germany. *Agric For Meteorol* 151:746–754
- Su H-B, Shaw R, Paw U K (2000) Two-point correlation analysis of neutrally stratified flow within and above a forest from Large-Eddy simulation. *Boundary-Layer Meteorol* 49:423–460
- Thom A (1975) *Vegetation and the atmosphere, vol 1: principles*, chap: Momentum, mass and heat exchange of plant communities. Academic Press, New York, , pp 57–109, 298 pp
- Vosselman G, Maas H-G (2010) *Airborne and terrestrial laser scanning*. Whittles Publishing, Dunbeath, 336 pp
- Wang W, Yi C (2012) A new nonlinear analytical model for canopy flow over a forested hill. *Theor Appl Climatol* 109:549–563
- Watanabe T (2009) LES study on the structure of coherent eddies inducing predominant perturbations in velocities in the roughness sublayer over plant canopies. *J Meteorol Soc Jpn* 87(1):39–56
- Weller G, Tabor G, Jasak H, Fureby C (1998) A tensorial approach to computational continuum mechanics using object-oriented techniques. *Comput Phys* 12(6):620–631
- Wilson J (1988) A second-order closure model for flow through vegetation. *Boundary-Layer Meteorol* 42:371–392
- Yang B, Morse A, Shaw R, Paw U K (2006a) Large-eddy simulation of turbulent flow across a forest edge. Part II: momentum and turbulent kinetic energy budgets. *Boundary-Layer Meteorol* 121:433–457
- Yang B, Raupach M, Shaw R, Paw U K, Morse A (2006b) Large-eddy simulation of turbulent flow across a forest edge. Part I: flow statistics. *Boundary-Layer Meteorol* 120:377–412
- Yang B, Shaw R, Paw U K (2006c) Wind loading on trees across a forest edge: a large eddy simulation. *Agric For Meteorol* 141:133–146
- Yue W, Parlange M, Meneveau C, Zhu W, van Hout R, Katz J (2007) Large-eddy simulation of plant canopy flows using plant-scale representation. *Boundary-Layer Meteorol* 124:183–203